Journal of
Medicinal Chemistry

Article

Monosaccharide Analogues of Anticancer Peptide R-lycosin-I: Role of Monosaccharide Conjugation in Complexation and Potential of Lung Cancer Targeting and Therapy

peng zhang, jing ma, qianqian zhang, shandong jian, xiaoliang sun, bobo liu, liqin nie, meiyan liu, Songping Liang, Youlin Zeng, and Zhonghua Liu

J. Med. Chem., **Just Accepted Manuscript** • DOI: 10.1021/acs.jmedchem.9b00634 • Publication Date (Web): 05 Jul 2019

Just Accepted

is published by the American Chemical Society. 1155 Sixteenth Street N.W., Washington, DC 20036

Monosaccharide Analogues of Anticancer Peptide R-lycosin-I: Role of Monosaccharide Conjugation in Complexation and Potential of Lung Cancer Targeting and Therapy

Peng Zhang[1,2†], Jing Ma[2†], Qianqian Zhang[1], Shandong Jian[1], Xiaoliang Sun[2], Bobo Liu[2], Liqin Nie[2], Meiyan Liu[2], Songping Liang[1], Youlin Zeng[2]* and Zhonghua Liu[1,3]*

1. The National &Local Joint Engineering Laboratory of Animal Peptide Drug Development, College of Life Sciences, Hunan Normal University, Changsha Hunan 410081, China. E-mail: liuzh@hunnu.edu.cn
2. The National and Local Joint Engineering Laboratory for New Petrochemical Materials and Fine Utilization of Resources, Hunan Normal University, Changsha Hunan 410081, China. E-mail: youlinzengcn@gmail.com
3. State Key Laboratory of Developmental Biology of Freshwater Fish, College of Life Sciences, Hunan Normal University, Changsha Hunan 410081, China

* Corresponding author

† These authors contribute equally to this paper.

Abstract

Glycoconjugation is a promising modification strategy for the optimization of peptide drugs. In this study, five different monosaccharides derivatives (**7a-e**) were covalently linked to *N*-terminal of R-lycosin-I, which yielded five glycopeptides (**8a-e**). They demonstrated increased or reduced cytotoxicity depending on monosaccharide types, which might be explained by the changes of physicochemical properties. Among all synthesized glycopeptides, only **8a** exhibited both increased cytotoxicity (IC_{50}=9.6±0.3 μM) and selectivity (IC_{50}=37.4±5.9μM). The glucose transporter 1(GLUT1) with high expression in cancer cells was approved to involve in the cytotoxicity and selectivity enhancement of **8a**. Furthermore, **8a** but not R-lycosin-I inhibited tumor growth in nude mice xenograft model without generating side effects by intraperitoneally. Taken together, this study revealed the different monosaccharide roles in peptide modification and also provides an optimized anticancer peptide with high activity and selectivity, that is, **8a** might be a promising lead for developing anticancer drugs.

Keyword: Glycoconjugation, anticancer peptides, R-lycosin-I, monosaccharide, xenograft model.

Introduction

Although there are a growing number of progress have been made in reducing incidence and mortality rates of cancers, cancers remain a major cause of mortality worldwide and further strategies for cancer treatment are needed[1-3]. Small cell lung cancer (SCLC) is an exceptionally lethal malignancy for which more effective therapies are urgently needed[4]. Cation anticancer peptides (ACPs) have been considered as novel therapeutic candidates due to their ability to kill target cells rapidly and low immunogenicity[5, 6]. However, their development as novel anticancer agents has been hampered by their lower cytotoxic activity especially in solid tumor, poor serum half-lives, and cytotoxicity to host[7, 8]. To address these problems, modification strategies have been applied to develop novel synthetic ACPs. There are two principally approaches used for ACP optimization[9]. (1) One approach is template modification. This strategy includes the systematic sequence truncation, amino acid substitution, hybridization and/or cyclization, which is characterized by using an active naturally occurring sequence as a starting "template"[9, 10]. Some studies demonstrated that amino acid substitutions and/or sequence truncations at peptide termini can enhance salt and serum stability[11-13], as well as reduce toxicities[14]. Our previous study showed that lysine substitution by arginine in the sequence of lycosin-I endows this peptide higher anticancer activity in solid tumors *in vitro* and *ex vivo*[15]. (2) The other one is conjugation of peptides with other materials including carbohydrate, PEG, fatty acid, photothermal materials *etc*[16-20]. Many studies show that this peptide modification strategy is promising in anticancer drug development. For example, photothermal material conjugation of ACPs has been found to improve anticancer activity and selectivity *in vitro* and *in vivo*[21].

Glycosylation is a naturally occurred process which has many functions, including affecting the fold, stability, localization, immunogenicity, activity of proteins and other macromolecules. Therefore, glycosylation is also an important parameter in the optimization of many protein and peptide drugs. For example, the approved cyclic peptide antifungal drug caspofungin conjugated with β-D-glucopyranose shows stronger and broader antifungal activity[22]; monosaccharide modification can also improve the antifungal activity of tunicyclin D[23]; the addition of sialyl LacNAc to GLP-1 greatly improves stability against DPP-IV and NEP 24.11 and extends the

blood glucose-lowering activity *in vivo* as compared to the native type[24]. Furthermore, the "Warburg effect"[25] explains why there are over expression of glucose-transporters in cancer cells and drastically increased glucose intake, which provides clinically validated targets for cancer treatment[26-28]. Therefore, researches regarding glycoconjugates for specific delivery of various radiotracers, fluorophores, and organic anticancer drugs have attracted many attentions. Studies indicate that multifarious anticancer drugs, for example, azomycin, adriamycin, paclitaxel, can be delivered specifically to cancer cells by covalently conjugating with carbohydrates[29]. Stephen J. Lippard group synthesized and characterized six positional isomers of glucose-platinum conjugates which exhibit different cellular uptake and cytotoxicity[30, 31]. This study also well reveals specific cancer targeting through glucose-transporter mediated uptake *in vitro* and *in vivo*. In addition to, by covalently conjugated with maltose, the chemical and biological activity of Eugenol were improved [32].

Our previous study demonstrated that R-lycosin-I, an analogue derived from the anticancer peptide lycosin-I, is a promise lead from the development of anticancer peptide drugs[15]. However，this peptide displays some drawbacks including low activity, selectivity and stability in serum. Considering the advantages of carbohydrate modification mentioned above, we made an attempt to optimize R-lycosin-I, that is, to improve its anticancer potential by conjugate monosaccharides to R-lycosin-I. In this study, five glycopeptides were synthesized and characterized by coupling monosaccharide derivatives **7a**, **7b**, **7c**, **7d** and **7e** to the *N*-terminal of R-lycosin-I named as **8a**, **8b**, **8c**, **8d** and **8e**, respectively. Compared with R-lycosin-I, they displayed stronger or weaker cytotoxic activities depending on monosaccharide types, which might be explained by the alteration of the physiochemical properties including size, zeta potential, secondary structure of the glycopeptides. Interestingly, **8a** showed not only higher cytotoxic activity but also higher selectivity against cancer cells. The glucose transporter GLUT1 which is high expressed in cancer cells might involve in this process. Furthermore, **8a** inhibited the tumor growth in *ex vivo* and *in vivo* experiments. Taken together, our study developed a physicochemical properties-activity relationship to describe the roles of different monosaccharides in the anticancer process, and provided clues and leads for the development of anticancer drugs with high efficacy and safety.

Results

Synthesis of R- lycosin-I-monosaccharide conjugates

Five monosaccharide derivatives, 3'-aminopropyl β-D-glucopyranoside (**7a**), 3'-aminopropyl β-D-galactopyranoside (**7b**), 3'-aminopropyl α-D-mannopyranoside (**7c**), 3'-aminopropyl α-L-arabinopyranoside (**7d**), 3'-aminopropyl 2-deoxy-2- acetamido-β-D-glucopyranoside (**7e**), were synthesized from monosaccharide by acetylation, 1-O-selective deacetylation, trichloroacetimidation, glycosylation, deprotection, and staudinger reaction (see **Experimental Section**, **Scheme 1-5**). The structures of target compounds and some synthetic intermediates were characterized by ^{1}H NMR and ^{13}C NMR. The NMR spectrums of monosaccharide derivatives were included in the Supporting Information Page S3-S8. The peptide R-lycosin-I was synthesized using the standard 9-fluorenyl-methoxycarbonyl (Fmoc) solid-phase peptide synthesis method. The monosaccharide derivative was conjugated to the *N*-terminal of R-lycosin-I with glutaric anhydride as the linker between the monosaccharide derivative and the peptide. The five monosaccharide derivatives (**7a**, **7b**, **7c**, **7d** and **7e**) were used to synthesize five glycopeptides, which were named as **8a**, **8b**, **8c**, **8d** and **8e,** respectively. As shown in Figure 1A-B, the synthetic **8a** and **8b** were purified by using prepared C18 RP-HPLC and analytical C18 RP-HPLC analysis indicated that the two synthetic glycopeptides all had high purity (Figure 1A-B, *inset*). So did the other three glycopeptides **8c**, **8d** and **8e** (Figure S1A-C). As the determined by MALDI-TOF MS, the average molecular masses were 3263.47 Da for **8a**, 3263.39 Da for **8b**, 3264.20 Da for **8c**, 3229.23 Da for **8d** and 3304.49 Da for **8e** (Figure 1C-D; Figure S1D-F), which were same as those of calculated ones based on the sequences, respectively. The data confirmed the successful synthesis of the five glycopepitdes. The fluorescein isothiocyanate (FITC) labeled **8a** was also synthesized by coupling FITC to the side chain amide group of the *N*-terminal lysine residue of R-lycosin-I (see Supporting Information Page S2).

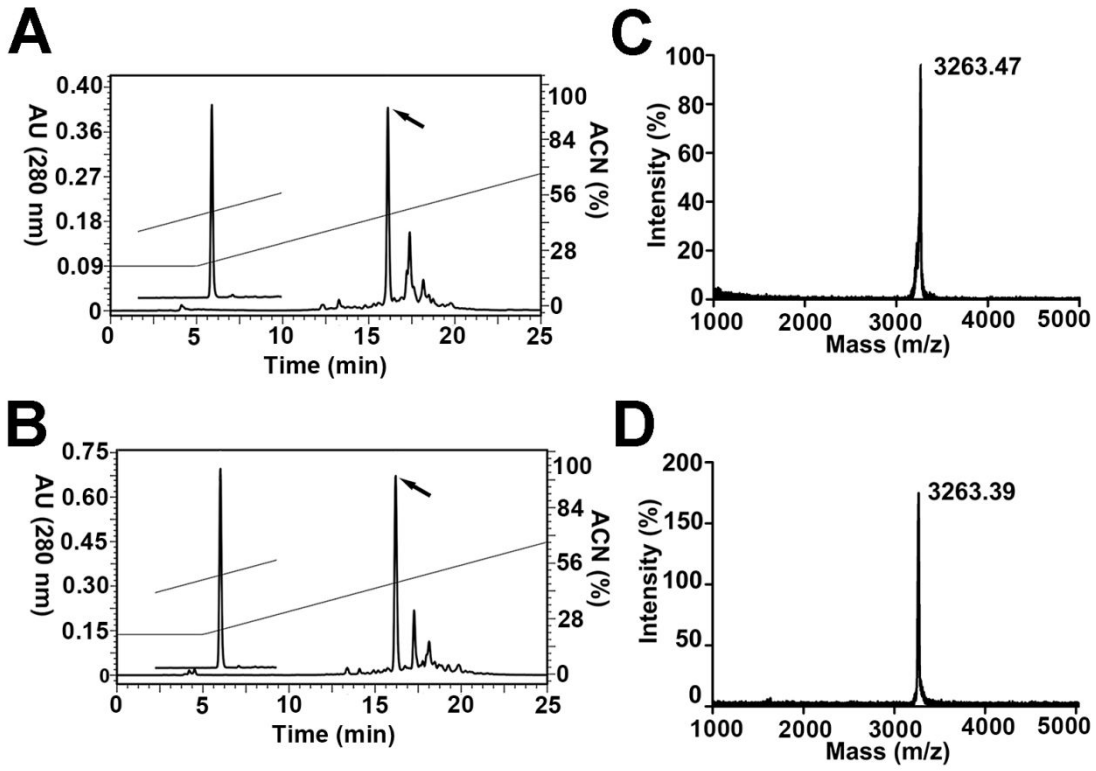

Figure 1. The purification and molecular mass determination of **8a** and **8b**. The purification of **8a** (A) and **8b** (B) by using RP-HPLC (column, Welch, C18, 300 Å, 10 × 250 mm). The synthetic glycopeptides were eluted using a linear acetonitrile gradient (0-80% acetonitrile/0.1% TFA) at a flow rate of 3.0 ml min^{-1}. The elution of the peptides was monitored at 280 nm. *Inset*, the purity of purified glycopeptides was analyzed by analytical RP-HPLC. The molecular masses of **8a** (C) and **8b** (D) were determined by MALDI-TOF MS.

Cytotoxicity profile of R-lycosin-I and their conjugates

The cytotoxic activity of the five glycopeptides was evaluated on human lung carcinoma cells (A549) and non-cancer cells (HEK-293T). The IC_{50} values were calculated to evaluate the potency of glycopeptides, which represent the concentrations of the glycopeptides that confer 50% growth inhibition of cells. As shown in Figure 2A, for A549 cells, the cytotoxic activities of the peptides were ranked as **8b** ≈ **8d** ≈ **8a** > R-lycosin-I > **8e** > **8c**; while for HEK-293T cells, those were ranked as **8b** > **8d** > R-lycosin-I > **8e** > **8a** > **8c**. These data indicated that **7b** and **7d** modification enhanced the cytotoxic activity of R-lycosin-I on both cell lines, while **7c** and **7e** modification resulted in reduction or loss of activity. It was interesting that **7a** coupling to the

N-terminal of R-lycosin-I had increased inhibition on A549 cancer cells but decreased effect on HEK-293T non-cancer cells, suggesting improved selectivity. In addition to CCK-8 assay, another cell viability assay also examined. Trypan blue is a cell-active dye that is commonly used to detect cell membrane integrity and is often used to detect cell survival. Live cells are not stained blue, and dead cells are dyed light blue. Therefore, according to the CCK-8 assay, we choose the IC_{50} value of R-lycosin-I and performed the trypan blue staining. As shown in Figure 2B and S2, when treated with 15 μM R-lycosin-I, about half of cells turned blue; cells treated with **8a**, **8b** and **8d** were basically stained blue and a few blues were observed to the **8c**, **8e** and control. Next, **8a** and **8b** were further applied in the expanded cytotoxicity tests. As shown in Table 1, **8b** exhibited high potency and inhibited cancer cell growth with IC_{50} values of 4-9 μM in cancer cell lines (MDA-MB-231, H460, H1437, HGC-27 and PC-3) and non-cancer cell lines (HEK-293T and L-02).The cytotoxic activity of **8a** against those cancer and non-cancer cell lines was 6.89-13.05 μM and 25.91-37.44 μM, respectively, unlike **7b,** further confirming that **7a** conjugation enhanced not only the cytotoxic activity but also the selectivity on cancer cells over non-cancer cells. The A549 cells and **8a** were chosen as the study subject in follow-up experiments. We further verified the effects of **8a** on cell proliferation by colony formation assay. Compared with control, the treatment group caused a strong inhibition of colony formation at the concentration of 4 μM **8a** (Figure 2C-D). The data indicated that **8a** could also inhibit cell growth at low concentration less than IC_{50} values. On the other hand, we measured if the glycopeptides triggered apoptosis of A549 cells using flow cytometry (Figure 2E). The percentage of apoptotic cells increased from 4.59 % in the control to about 40.16 % in **8a**-treated A549 cells at the concentration of 8 μM, respectively. However, the 8 μM R-lycosin-I treatment did not cause obvious apoptotic effect on A549 cells. These results indicated monosaccharide conjugation to the N-terminal of R-lycosin I could incearse or reduce the cytototoxic activity of the peptide depending on the monosaccharide types.Note that damage to the integrity of the cell membrane also causes Annexin V to be colored. So, in order to accurately exam the apoptosis, the caspase-3 activity was performed as described blow. For the **8a**, in low concentration, its cytotoxic activity may be derived from the proliferation inhibition and apoptosis inducement. These results indicated monosaccharide conjugation to the N-terminal of R-lycosin-I could incearse or reduce the cytotoxic activity of the peptide depending on the monosaccharide types.

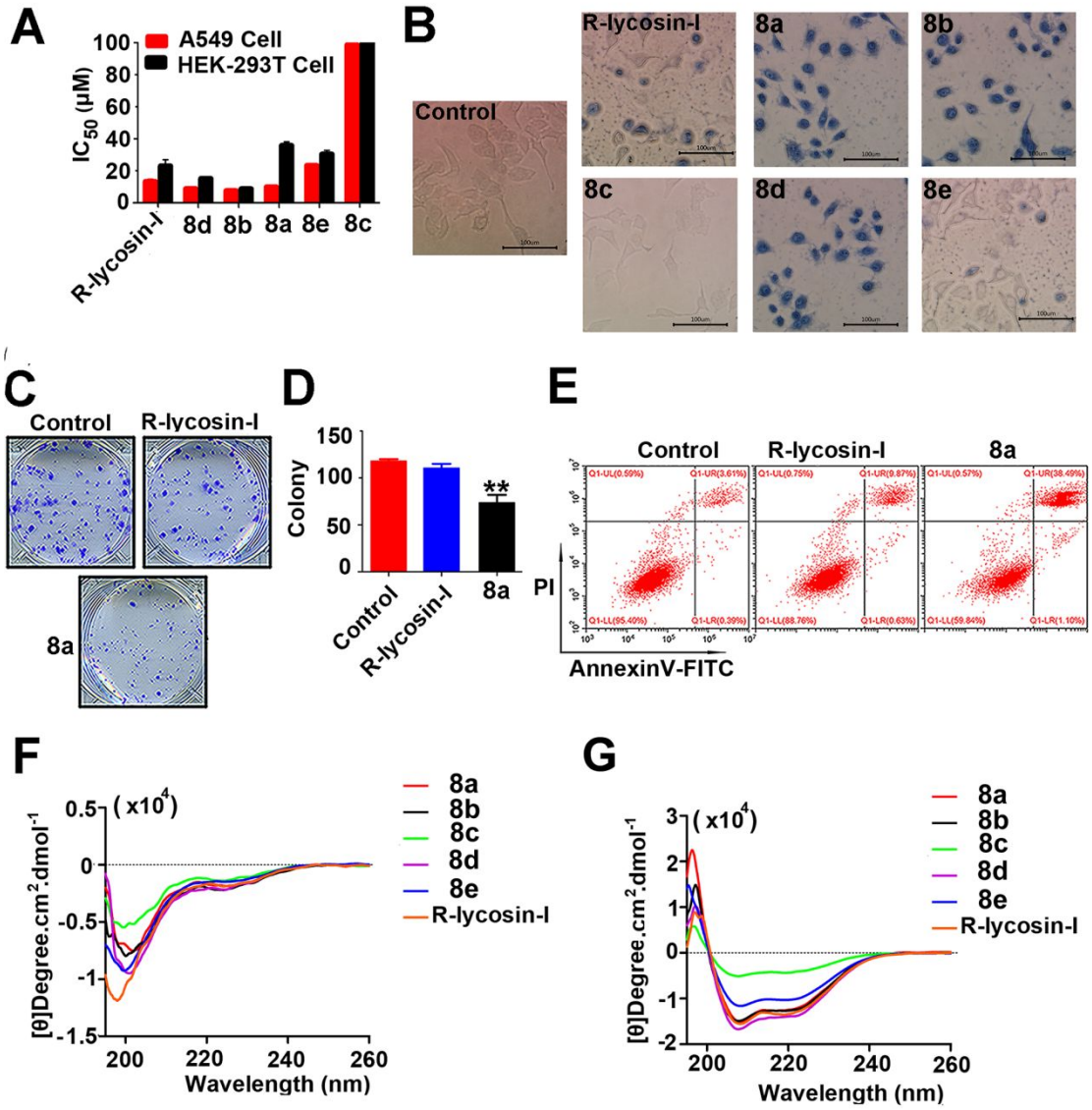

Figure 2. The cytotoxic activities of R-lycosin-I and five glycopeptides. (A) The IC_{50} values of the six peptides on A549 and HEK-293T cells as determined by CCK-8 assay. IC_{50} value was determined by averaging three repeated experiments. Each experiment consisted of 3 repetitions. (B) Trypan blue staining of 5glycopeptides and R-lycosin-I. (C) Colony formation viability of A549 cells treated with 4 μM R-lycosin-I and **8a** were evaluated by clonogenic assay. (D) Quantitative results are illustrated for clonogenic assay, (n=3). (E) Cell apoptosis in A549 cells treated with 8 μM R-lycosin-I and **8a** determined by flow cytometry. The circular dichroism spectra of R-lycosin-I and glycopeptides. (E) In the presence of 50% TFE at 25 °C. (F) In benign medium (PBS) at 25 °C. (G) The morphology of R-lycosin-I and glycopeptides analyzed using TEM.

Table 1 Cytotoxic activity (IC_{50}) activities of peptides against non-cancer cells and cancer cells.

Peptides	IC_{50} (μM)							
	HEK-293T	L-02	MDA-MB-231	A549	H460	H1437	HGC-27	PC-3
R-lycosin-I	25.8±3.7	12.6±1.1	10.5±0.5	14.3±1.3	12.9±1.3	16.5±1.3	12.5±1.2	15.6±0.6
8a	37.4±5.9	25.9±3.8	10.1±0.2	9.6±0.3	8.5±0.4	13.0±0.2	12.6±0.6	6.9±0.4
8b	8.3±0.4	4.8±0.3	6.0±0.2	7.0±0.3	4.9±0.9	5.3±0.2	5.3±0.2	4.9±0.2

IC_{50} value (μM) represents the concentration of a certain peptide at which cell viability was inhibited by 50% in comparison with the untreated cells. IC_{50} value was determined by averaging three repeated experiments. Each experiment consists of 3 repetitions.

Physicochemical characteristics of glycopeptides

Some physicochemical parameters such as shape, size, surface charge, hydrophobicity, secondary structure, are known to play important roles in cytotoxic activity of ACPs[18]. Therefore, we assumed that the varied cytotoxic activities of the glycopeptides might in part be related to the parameter changes which were resulted from the conjugation of different monosaccharides. The TEM analysis showed that all of the six peptides were spherical in shape with a diameter of ~80-150 nm (Figure S3). As shown in Table 2, all the peptides had similar hydrophobicity as represented by retention time in RP-HPLC analysis, except that **8e** had slightly higher hydrophobicity; the sizes, surface charges and helicities of R-lycosin-I were all affected by the monosaccharide modification. The zeta potentials are +26.13±3.45 mV for R-lycosin-I, +25.9±1.24 mV for **8a**, +50.43±2.94 mV for **8b**, +3.81±1.02 mV for **8c**, +35.73±7.24 mV for **8d**, and+9.66±2.03 mV for **8e**. The hydrodynamic sizes as determined by DLS are 252.77±28.25 nm (Polymer dispersity index (PDI) = 0.601±0.033) for R-lycosin-I, 471.67±74.28 nm (PDI = 0.689 ±0.028) for **8a**, 232.30±14.23 nm (PDI = 0.259±0.016) for **8b**, 1101.00±80.89 nm (PDI = 1.000) for **8c**, 222.57±9.73 nm (PDI = 0.458±0.071) for **8d**, and 696.70±45.01 nm (PDI=0.919±0.062) for **8e**. Same as R-lycosin-I, the five glycopeptides adopted random coil conformation in PBS buffer and alpha-helical conformation in 50% TFE as determined by CD (Figure 2 F -G). As compared with R-lycosin-I, **8d** displayed a perfect α-helical structure, **8a** and **8b** had similar helicities, **8e** had reduced helicities, whereas **7c** modification drastically disrupted the stabilization of the α-helix conformation of R-lycosin-I (Table 2).

It has been accepted that the cytotoxic activity of ACPs was affected by multi-factors. Most

ACPs are positively charged, which may facilitate the electrostatic attraction between ACPs and the negatively charged components of the membrane of cancer cells. Because cancer cell surface contains more negatively charged components than that of non-cancer cells, the positive charges of ACPs are believed to be important to their selective action on cancer cells over non-cancer cells[33]. The zeta potential which is considered strongly cationic when the value is greater than +30 mV[34]. The strongly cationic particles generally displaying stronger toxicity associated with cell membrane disruption, which may cause peptide loss of selectivity. The size effect proposed by Zheng *et al*. indicated that relatively smaller particle size is more likely to be taken up by cells[35]. The increased hydrodynamic size may result from peptide self-association in aqueous solutions[36, 37], which may decrease the ability of the peptide to dissociate, and penetrate into the cytoplasmic membrane to kill cells[38]. In addition， amphipathic helical conformation is often required to the cytotoxic activity of ACPs.

With these determined parameters, we attempted to establish the relationship between the cytotoxicity potency and these parameters of the peptides. Accordingly, the five glycopeptides could be classified into three groups. (1) **8b** and **8d**. Their increased activity might closely correlated with their sharply increased net positive charges， reduced hydrodynamic sizes and high helicities, which might even cause their loss of selectivity on cancer and non-cancer cells. (2) **8c** and **8e**. It was evident that their low activity might be derived from their reduced net charges, greatly increased hydrodynamic sizes and most importantly low helicity. These parameters might function in a combination way. The large sizes of **8c** and **8e** might be resulted from their self-association in aqueous because of small net charges and low helicities. (3) **8a**. It displayed unchanged net charges, increased hydrodynamic size and high helicity. It seems that these changes could not explain the increased activity and selectivity of **8a**. Therefore, beside the physicochemical characteristics, some biological properties would be involved, which would be described as below.

Table 2 Physicochemical parameters of R-lycosin-I and glycopeptides

Peptides	Zeta potential (mv)	Average sizes (nm)	PDI	Hydrophobicity[a] $t_{R\ (min)}$	Benign		50% TFE	
					$[\theta]_{222}$[b]	% Helix[c]	$[\theta]222$[b]	% Helix[c]
R-lycosin-I	+26.13±3.45	252.77±28.25	0.601±0.033	15.14	-1724.82	12.48	-12911.59	93.54
8a	+25.90±1.24	471.67±74.28	0.689±0.028	15.87	-1830.29	13.50	-12143.39	89.64
8b	+50.43±2.94	232.30±14.23	0.259±0.016	15.96	-2186.47	15.53	-12373.36	87.92
8c	+3.81±1.02	1101.00±80.89	1.000	15.58	-1380.73	9.94	-4090.38	29.60
8d	+35.73±7.24	222.57±9.73	0.458±0.071	15.43	-2057.99	14.97	-13807.07	100.00
8e	+9.66±2.03	696.70±45.01	0.919±0.062	17.80	-1455.69	10.57	-10083.70	73.00

[a] The overall hydrophobicity was represented by retention time (t_R) by RP-HPLC at room temperature.
[b] The mean 222 values (in deg.cm^2.dmol^{-1}) at wavelength 222 nm were measured at 25°C by circular dichroism spectroscopy.
[c] The helical content (in percent) of a peptide is relative to the molar ellipticity value of the peptide.

Intracellular distribution and cellular uptake analysis

Our previous study indicated that R-lycosin-I can interact with cell membrane and penetrate cell membrane to locate in cytoplasm. We wonder whether **7a** modification would affect such an effect of R-lycosin-I. In order to precisely locate **8a** in A549 cells, the fluorescence distribution of FITC-modified **8a** in cells was visualized using laser confocal microscopy after 2 h incubation at the concentration of 15 μM. As shown in Figure 3A, the two peptides were observed inside A549 cells, but there were differences regarding their distribution in cells. First, FITC-R-lycosin-I exhibited granular-like distribution in the cytoplasm, may be because some R-lycosin-I molecules still accumulated in granular structures in cytoplasm when entering inside cells. Compared to R-lycosin-I, **8a** relatively dispersed and equally distributed in the cytoplasm, as observed for histidine-rich peptides Ctry2459-H2 and Ctry2459-H3[39], indicating that they could escape from vesicles more easily than R-lycosin-I, which might account for their enhanced cytotoxic activity. Second, the fluorescent signals of **8a** but not R-lycosin-I were found to be aggregated in the cell nucleus, indicating that monosaccharide modification could significantly enhance the ability of the peptide to penetrate membrane including the nuclear envelope (NE). It was reported that after translocation into cell nucleus, the peptide, Azurin, would interact with nucleus targets, such as P53, triggering cell apoptosis[40]. In this respect, **8a** may enhance the NE penetration to improve the cytotoxic activity.

Next, we determined that the effect of **7a** on the cellular uptake of R-lycosin-I. As shown in Figure

3B-C, for R-lycosin-I at low concentration of 6.25 μM, long time treatment could not lead to the increment of fluorescent cells. When the concentration of the peptides was increased from 6.25 μM to 12.5 μM, the number of fluorescent cells would increase by 2-3 times. At the same concentration (6.25 μM or 12.5 μM) or time point, **8a** demonstrated significantly higher cell uptake capacity than R-lycosin-I, consistent with their higher cytotoxic activity on A549 cells than R-lycosin-I. These data implied that their cytotoxicity potency might be positively correlated with their cell uptake capacity.

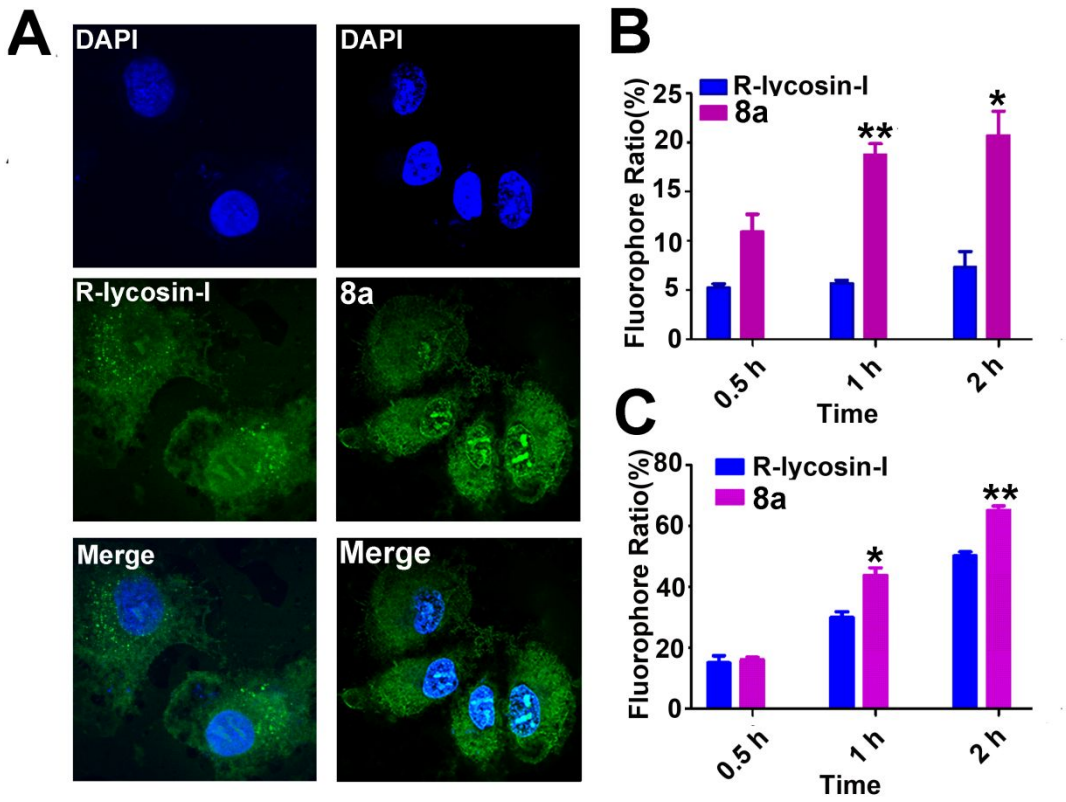

Figure 3. Cellular distribution and cell uptake ratio of R-lycosin-I and **8a**. (A) Peptides distribution in A549 cells examined by laser scanning confocal microscopy. (C and D) Quantitative comparison of cellular uptake of R-lycosin-I and **8a** at the concentration of 6.25 μM (C) and 12.5 μM (D), respectively, (n=3). The number of fluorescence-labeled cells was counted using Cellometer K2. The scale bar represents 50 μm.

Glucose-transporter mediated cytotoxic activity of 8a

It was interesting that **8a** demonstrated much higher selectivity on cancer cells over non-cancer cells than R-lycosin-I and **8b**. However, this seem cannot be explained by chemical

and biological properties mentioned above. It has been accepted that glucose transporter 1 (GLUT1) is broadly over-expressed in many different cancers[41], which provides a good surface receptor for selectively targeting cancer cells[42]. Therefore, we wondered if the high expression of GLUT1 on cancer cells contributed to the enhanced selectivity of **8a** through **7a** and GLUT1 interaction. Firstly, the cytotoxic activity of the **8a** was determined in the absence and presence of the GLUT1 inhibitor STF-31 on A549 cells. As shown in Figure 4A, the cell viability of A549 cells treated with 12.5 μM **8a** was proximately 54% and 40% (P<0.05) in the absence and presence of STF-31 treatment, respectively. However, there was no obvious difference when A549 cells treated with 12.5 μM R-lycosin-I, **8b** and **8d** (Figure S4A) in the presence and absence of STF-31. In addition, LDH assay performed to exam the selectively penetration of cancer cell and non-cancer cell membrane when treated with 12.5 μM **8a**, **8b** and **8d** which showed enhanced cytotoxicity compared to R-lycosin-I. As shown in Figure S4B, this result demonstrated that only the **8a** had selectivity.

Next, when GLUT1 expression in A549 cells was knocked down by RNAi, the cytotoxic activity of **8a** on A549 cells was accordingly reduced. Compared with control oligos, GLUT1 RNAi oligos led to approximately 50 % knockdown of GLUT1 expression in A549 cells (Figure 4B; Table S1), which made the IC_{50} value of **8a** increased by 1.4 folds (13.4 μM in A549 cells with low GLUT1 expression vs 9.9 μM in cells with normal GLUT1 expression) (Figure 4D). Accordingly, the cellular uptake of FITC-**8a** was also significantly reduced in response to knock down of GLUT1 expression in A549 cells (Figure 5E). In addition, HEK293T cells exhibited lower GLUT1 expression than A549 cells (Figure 4C). These data indicated that the high expression level of GLUT1 in cancer cells might be related to the selective cytotoxic activity of **8a**.

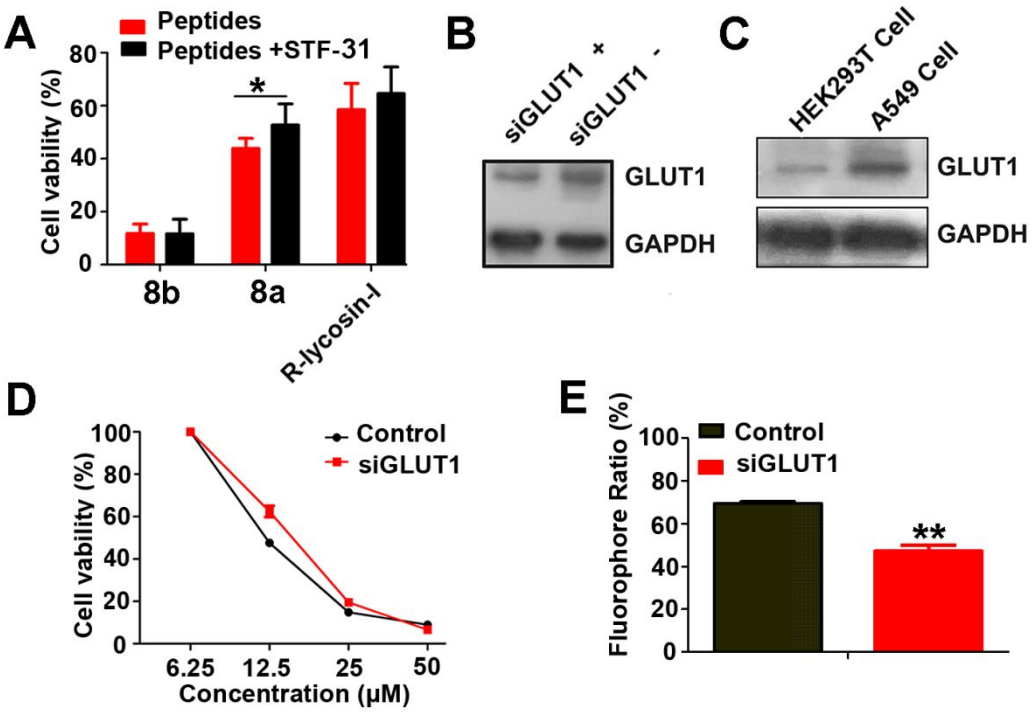

Figure 4. Glucose-transporter mediated cytotoxic activity of **8a**

(A) Effect of GLUT1 inhibitor STF-31 on the cytotoxic activity of R-lycosin-I, **8a** and **8b**. A549 cells were pre-incubated with 1 μM STF-31 for 4 hours and then treated with 12.5 μM peptides for 2 h. (B and C) Western blot analysis of GLUT1 expression in A549cells and HEK293T cells. (D) Representative dose-response curves for A549 and A549-GLUT1 RNAi cells treated with a series of concentrations of **8a**. (E) The cellular uptake of FITC-**8a** in A549 and A549-GLUT1 RNAi cells, respectively at the concentration of 12.5 μM for the exposure time of 2 h, (n=3).

Mechanism underlying the cytotoxic activity of 8a

As mentioned above, the two peptides, R-lycosin-I and **8a**, could bind to cell surface and enter into the interior of A549 cells, which could induce cell death. The binding of the peptides to cell surface result in cell membrane disruption. Actually, this is a common mechanism shared by most ACPs[43]. SEM examination was applied to observe the effect of **8a** on cell morphology. Untreated A549 cells showed plump spindle cell morphology (Figure 5A). In contrast, A549 cells treated with 15 μM R-lycosin-I (Figure S5A) and **8a** (Figure 5B) for 24 h showed marked alterations in cell morphology. Mostly shrunken cells with membrane disruption and lysis were observed. The release of lactate dehydrogenase (LDH) was widely used to measure membrane

integrity.[44] The peptide treatment indeed led to LDH release from A549 cells. An obvious release occurred at the peptide concentration near IC_{50} value of the corresponding peptide. For example, considering 1% TritonX-100 caused 100% release of LDH from A549 cells, the incubation of 12.5 μM **8a** or R-lycosin-I for 2 hours resulted in more than 30 % LDH release, respectively, indicating the rapid permeabilizing effect on the cancer cell membranes (Figure 5D). With the increasing of peptide concentration, more LDH release was observed, indicating more membrane permeabilization. These data suggested that rapid membrane disruption or membrane-lytic activity should be one of the mechanisms underlying these peptides inducing cell death.

In addition, some cells seem presented apoptosis bodies and severe surface bubbling (Figure 5C and Figure S5B), a characteristic event during the execution phase of cell apoptosis[45]. Considering mitochondrion plays a central part in cell apoptosis and many crucial factors and events in apoptotic death are regulated by it[46], the interaction of **8a** with mitochondrion was determined by co-localization assays. Expectably, the merge images showed overlapping between signals of FITC-labeled peptides and Mito-Tracker red (Figure 5E), which indicated that **8a** could be localized to mitochondria and implied that mitochondria-mediated cell apoptosis pathway might be involved[47]. Mitochondrial membrane potential (MMP) measurement demonstrated that the treatment with 15 μM peptides caused a significant loss of MMP in A549 cells (Figure 5F-G). Accordingly, MMP depolarization is often accompanied with increasing mitochondrial membrane permeability and Cytochrome C (CytC) release[48]. Therefore, immuno-fluorescence imaging was performed according to the method reported by chen C *et.al*[49]. As shown in Figure 5H, CytC in A549 cells displayed clear, grainy staining distribution in control cells, in contrast to diffuse staining in the cells treated with 15 μM peptides, indicating the transportation of mitochondria Cyt-C to cytoplasm. The released CytC further activates caspase cascade reaction and triggers cell apoptosis.[50] The caspase 3 activity was therefore examined using the specific protease-peptide substrate chromomeric reaction due to the caspase 3 activation was known as an effector of apoptotic pathways.[51] When treated with peptides, respectively, the caspase 3 activities in A549 cells were elevated by approximately 1.5-fold compared with the control (Figure 5I). These data indicated that **8a** brought about apoptosis of A549 cells through mitochondria-mediated pathway. These results mentioned above characteristically demonstrated that **8a** could initiate cell

membrane disruption and mitochondria-dependent apoptotic pathway, then synergistically achieving maximized cytotoxicity efficacy.

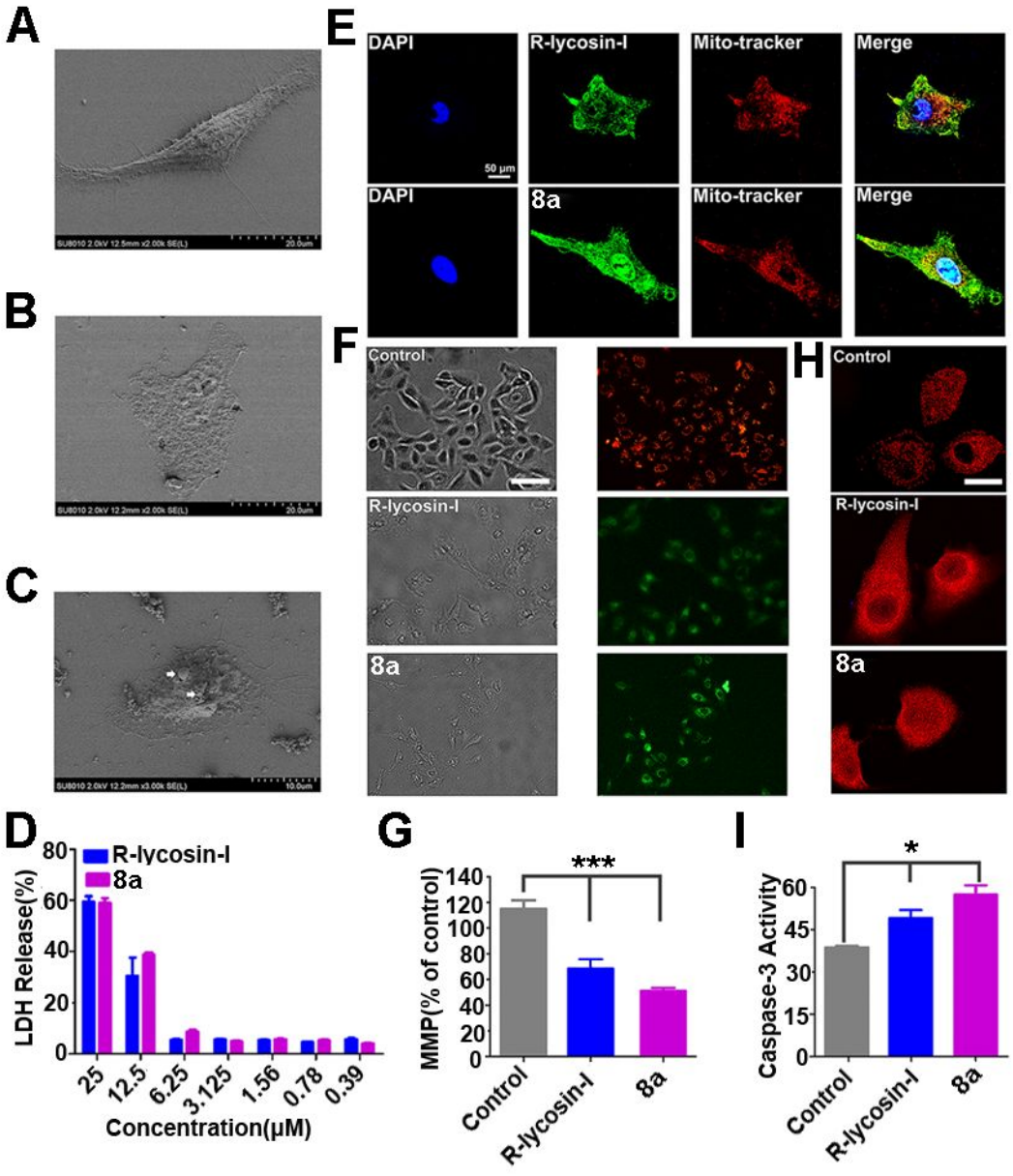

Figure 5. 8a caused direct cell membrane disruption and cell apoptosis. Representative SEM micrograph of A549 cells in control (A) or treated with 15 μM **8a** (B and C) for 24 h. (D) LDH leakage in A549 cells after treatment with R-lycosin-I and **8a** for 2h, respectively, (n=3). (E) Co-localization with mitochondria after treatment with FITC-labeled peptides for 24 h. Nuclei (blue color) and mitochondria (red color) were stained with DAPI and Mito-Tracker Red, respectively. (F) Fluorescent images of MMP staining with JC-1 in A549 cells before and after incubation with 15 μM R-lycosin-I and **8a** for 24 h, respectively. (G) Quantitative analysis of

MMP in A549 cells treated with R-lycosin-I and **8a** respectively, (n=3). (H) Immuno-fluorescence staining of CytC in A549 cells before and after treatment with 15 μM R-lycosin-I and **8a** for 24 h, respectively. (I) Caspase-3 activity in A549 cells before and after treatment with 15 μM R-lycosin-I and **8a** for 24 h, respectively, (n=3). The scale bar represents 100 μm.

***Ex vivo* antitumor performance**

Overwhelming evidences approve that *ex vivo* 3D tumor model more accurately reflects the morphology, growth kinetics, and protein expression profile of human tumors than simple two-dimensional cell monolayer.[52] Therefore, we performed a series of experiments to evaluate the activity of R-lycosin-I and **8a** on 3D tumor spheroids of A549 cells. Studies showed that penetration into tumor spheroids is required for the inhibitory activity of anticancer drugs.[53] First, we examined the penetration ability of the two peptides. A549 3D tumor spheroids were cultured with 30 μM FITC-modified peptides for 2 h and the FITC-fluorescence was determined by laser confocal microscopy using Z scan model (Figure 6A). In the 24 μm layer of the tumor spheroids treated with R-lycosin-I, no green fluorescence was detected in the center of the tumor spheroids, indicating that it might penetrate into the spheroids less than 16 μm in distance. However, when treated tumor spheroids with 30 μM **8a**, green fluorescence was detected even in the 48 μm layer, showing that monosaccharide modification markedly improved the peptide penetration ability into 3D tumor spheroids.

Next, in order to evaluate the activity of the two peptides on the tumor spheroids, A549 3D tumor spheroids were treated with the peptides at the concentration of 30 μM for six days, which were added three times, at day 0, day2 and Day 4. As shown in Figure 6B, in the control group, spheroids were gradually growing and generated tight spheroids, but looser morphology, physical shrinking and dissociation of the three-dimensional structure were observed in the peptide treatment groups. Note more evident changes were observed in **8a** groups than these of R-lycosin-I group, which was consistent with the tumor spheroid volume measurement and comparison (Figure 6C).

Finally, the cell viability of tumor spheroids in the **8a** groups was significantly lower than those observed for the control and R-lycosin-I groups, as revealed by the CCK-8 cytotoxicity

assay (Figure 6D). The increased activity of **8a** might be due to the improved cytotoxicity in two-dimensional cell monolayer, higher stability in serum (described below), and more effective penetration into the tumor spheroids. Given the relatively superior performance on the 3D tumor spheroids, we further performed *in vivo* animal model test.

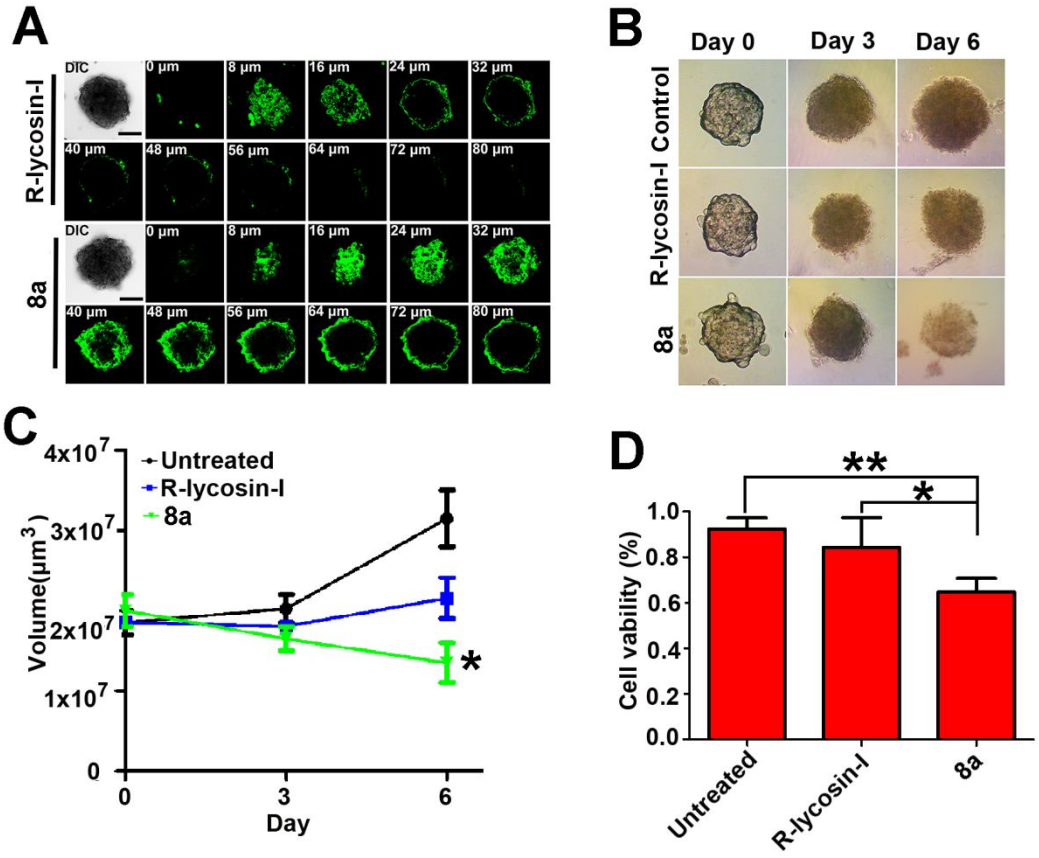

Figure 6. The effect of R-lycosin-I and **8a** on the 3D tumor spheroids of A549 cells. (A) The Z-stack confocal microscopy images of the A549 3D tumor spheroids treated with FITC-modified R-lycosin-I and **8a** at a concentration of 30 μM for 2 h, respectively. The spheroids were imaged using an Olympus FV1000 confocal microscope, preceding every 8 μm. Scale bar: 100 μm. The tumor spheroids size images(B), volume (C), and cell viability (D), were obtained in the presence 30 μM R-lycosin-I and **8a**, respectively, (n=3). The scale bar represents 100 μm.

Effect of 8a on inhibiting tumor growth in nude xenograft mice

The *in vivo* antitumor activities of R-lycosin-I and **8a** were investigated using the A549-luciferase xenograft model of lung cancer in nude mice[54]. R-lycosin-I and **8a** had the same

cytotoxic activity on A549-luciferase cells as on A549 cells used above (Figure S6). The lung tumor xenograft models of mice injected with **8a** showed strong fluorescent signals around tumor with 6 h post-injection (Fig. 7A). Compared with FITC treatment which had an extensive distribution in kidney and lung, the fluorescence of peptides treatment was detected in the liver, with minimal in the spleen and no detectable activity in the heart. Two weeks after implantation of A549-luciferase cells, the average tumor volume reached 150-180 mm^3. R-lycosin-I and **8a** were intraperitoneally injected every two days at the dose of 9 mg/kg. At day 14, significant inhibition of tumor growth was found in the **8a** treatment group as revealed by bioluminescent imaging, as compared with R-lycosin-I and PBS control groups (Figure 7B, *upper*). Furthermore, as shown in Figure 7C, a certain degree of inhibition of tumor growth was observed in R-lycosin-I treatment group compared to the control group, but only **8a** had a significant tumor volume reduction. On the other hand, if the two peptides were administrated by intratumor injection, a significant inhibition in tumor growth was observed during the course of experiments in mice treated with the two peptides at the dose of 3 mg/kg (Figure 7B, *lower* and 7D). In the way of intratumor administration, due to the drug can reach the tumor directly without blood circulation and there are only 1.6 times of cytotoxicity between R-lycosin-I and **8a** on A549 cells, R-lycosin-I and 8a showed similar activity to inhibit A549-luciferase tumor xenograft growth in vivo. It was noteworthy that no significant body weight changes were observed whether in intraperitoneal or intratumor treatments, indicating that these peptides did not diminish their overall health (Figure 7E-F). H&E staining showed no obvious changes in the primary organs (heart, liver and kidney) after treatment with the two peptides, indicating no potential toxicity of the two peptides to these organs (Figure 7G). In addition, our data indicated that **8a** is stable in serum and retained approximately 80% of its inhibitory activity in the exist of 10% serum within 48 hours, but R-lycosin-I was lack of most activity within 24 hours (Figure S7). This result indicated that the **8a** have higher serum stability than R-lycosin-I that will facilitate the enrichment of more **8a** at the tumor. Furthermore, TUNEL assays demonstrated much more apoptotic cells in the tumor tissues of **8a** group compared with those of groups (Figure 7H). All data above confirmed the *in vivo* anticancer activity of the two peptides, but only **8a** possessed efficacy in both intratumor and intraperitoneal injections.

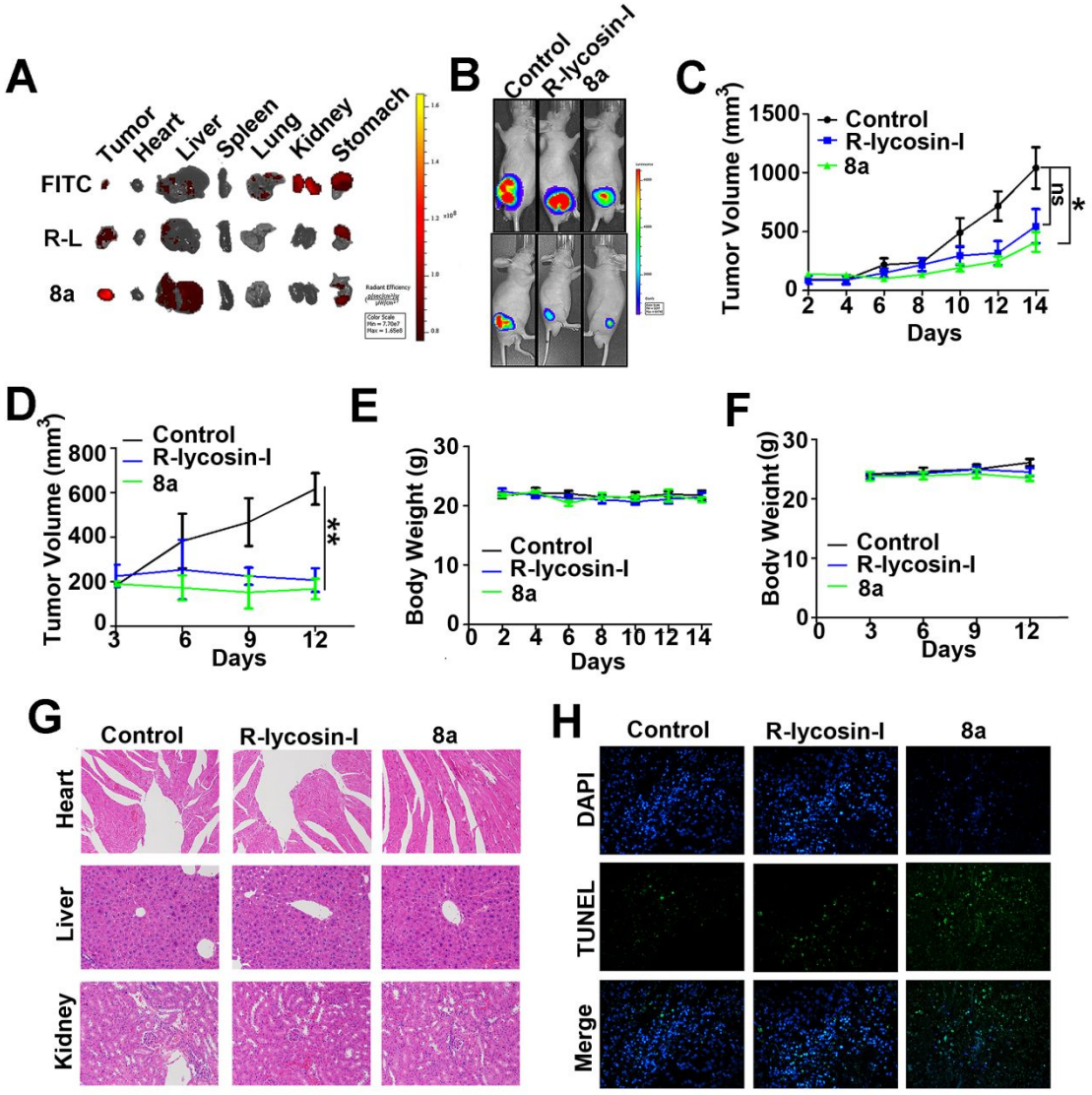

Figure 7. R-lycosin-I and **8a** inhibited A549-luciferase tumor xenograft growth in vivo. (A) Representative ex vivo fluorescence image of organs isolated from the animals after 6 hours administration of peptides; R-L represents the anticancer peptide R-lycosin-I. (B)bio-luminescent imaging on A549-luciferase tumor-bearing mice at the final day after 14 days for intraperitoneal (upper) and 12 days for intratumor injection (lower). (C)Tumor inhibition curves for intraperitoneal injection (n=5). (D) Tumor inhibition curves for intratumor injection (n=5). (E)Toxicity analysis by monitoring body weight after the peptide administration for intraperitoneal injection. (F) Toxicity analysis by monitoring body weight after the peptide administration for intratumor injection. (G) H&E assay for mice heart, liver and kidney tissues. The treatments were administrated via the intraperitoneal every other day for seven total times. (H)TUNEL assay for

mice tumor tissues. The treatments were administrated via the intraperitoneal every other day for seven total times.

Discussion and conclusions

An unprecedented number of marketing approvals (6 peptides) have witnessed a resurgence of peptide drug development which has greatly inspired the researchers[55]. The anticancer peptides (ACPs) have been described as promising molecules to treat cancer cells due to their kill target cells rapidly, broad spectrum activity and hardly to develop resistance[56-58]. Except those extraordinary properties, several obstacles have also appeared in development of peptide-based drugs for example poor pharmacokinetics, low cytotoxic activity to solid tumor and lack of selectivity[59]. Some strategies have been attempted to develop peptide molecules with optimal therapeutic index in the anticancer field. Strategies such as combination therapy[60], peptide template modification[61] and covalent coupling modification[62] can immensely improve the peptide performance. Among them, glycoconjugation is one of effective modification method for the optimization of anticancer drugs including serum stability enhancement, tumor targeting improvement and cytotoxicity increased[30]. Here, five glycopeptides were produced by covalently linked different monosaccharides (**7a-e**) to the *N*-terminal of R-lycosin-I. This article is mainly from two aspects to expound the research of glycoconjugation.

One aspect is significance of glycosylation as a strategy to enhance the selectivity and cytotoxicity of ACPs. Cytotoxicity assay including CCK-8 and trypan blue staining were used to measure the cytotoxic activity or selectively of 5 glycopeptides in cancer cell lines. In the paper, we used some cell lines in our laboratory as cytotoxicity test subject to make the conclusion of the change of cytotoxicity profile. Actually, there are many kinds of cell lines, and it is more difficult to test all of them with 5 glycopeptides which indicated that other cells may not have the equal behavior as the A549 and HEK293T. The result in Table 2 also demonstrated glycopeptides exhibit different cytotoxic activities against various cell lines. The primary target of most ACPs is cell membrane, and the interactions between cells and ACPs or the inherent membrane constitutions between cancer cells and non-cancer cells provide a valuable information and an opportunity to optimize the ACPs. It is well accepted that the cytotoxicity and selectively of ACPs are determined by numerous factors such as shape, size, surface charge, hydrophobicity, and

secondary structure[63] and the main mechanism of ACPs induce the cell death is destabilizing the membrane through multistep process[43]. Systematic combined physicochemical and biological properties to explain various cytotoxicity after monosaccharide conjugation provides a better understanding of the relationship between these factors and it also provides an effectively information to modify such peptide. Glucose transporter 1 (GLUT1) is broadly over-expressed in many different cancers, which provides a good surface receptor for selectively targeting cancer cells. The improvement selectively of **8a** closely related to the expression of GLUT1 cancer cell and non-cancer cell (Figure 4C). The glucose transporter uptake (Figure 4A) and internalization (data not shown) synergistically increased cell uptake of **8a**. The way **8a** was taken up by cells is diverse due to it contains both monosaccharides and peptide elements. The former may not only facilitate **8a** binding to GLUT1 to enhance its enrichment on the membrane and then internalization by the cells but also increase the glucose transporter uptake. Due to ACPs exert the cytotoxicity via a membrane disruption mechanisms only when its binds to the membrane to a 'critical' concentration[43], the enhanced cytotoxicity and selectivity might be explained as follows: the higher expression level of GLUT1 might attract more **8a** molecules to accumulate on the surface of cancer cells; consequently, **8a** might form a relatively higher concentration on cancer cell surface and then for cancer cells tend to induce cell death at a relatively lower concentration in solution than that for non-cancer cells.

Another aspect is efforts in the identification of **8a** as potential lead for anti-cancer drug development. Our previous data showed R-lycosin-I could inhibit cancer cells growth though mitochondria-mediated cell death pathway[15]. Accordingly, a series experiments including MMP measurement, cyt C release and caspase-3 activity detection (Figure 5F-I) verified that the mitochondria-dependent apoptotic pathway was also involved in **8a** treatment. Notably, rapid membrane disruption or membrane-lytic activity were appeared (Figure 5A-D) which is the main mode of action in **8a** brought about cell death and this mechanism was confirmed in majority ACPs. Due to **8a** exhibited relatively superior performance on the 3D tumor spheroids which more accurately reflects the real status of tumors than cell monolayer, in vivo animal model was performed to assess the anticancer potential of the molecule. Significant tumor volume reduction was observed in **8a** not in R-lycosin-I treatment group by intraperitoneally. The highest

bio-stability in serum is crucial for the in vivo therapeutic effects of drugs. It has been reported that glycosylation modification can enhance the bio-stability of peptides[64]. The data could explain the low efficacy of R-lycosin-I in vivo. It has been reported that particles with zeta potentials outside of the range of -30 mV to +30 mV are prone to opsonization, leading to recognition and clearance by mononuclear phagocyte system[65], it seemed that **8a** did not probably undergo such clearance because of its moderate zeta potential. Furthermore, **8a** was able to target GLUT1 whose expression is high in cancer cells, making **8a** tend to accumulate in cancer tissue, uptake by tumor cells and then suppress tumor growth efficiently. However, the fact that these tumors by intratumor treatments were not completely eradicated and these tumors volume by intraperitoneal treatments were also constantly growing although smaller volume than the control can be explained in difficulties to diffuse through the necrotic area and relatively fast clearance of the peptides from the tumor site[66]. Therefore, further modification the **8a** with more therapeutic index to make it clinically applicable is our research focus in the next step.

In summary, the goal of this study is to improve the anticancer potential of R-lycosin-I. Five peptide-monosaccharide conjugates were synthesized and characterized. Fortunately, it was found that **7a** conjugation rendered R-lycosin-I higher cytotoxic activity and selectivity, two important parameters for therapeutic development of ACPs. The anticancer potential of **8a** was derived from the data at three levels, cell assay, 3D tumor spheroids and animal tumor models. Compared with R-lycosin-I, **8a** displayed more potent cell penetrating ability, which makes more **8a** molecules distributed inside cancer cells and subsequently causes more cell death. Direct cell membrane disruption and mitochondria-mediated cell apoptosis were involved in the cell death induced by **8a**. We also found that glucose transporter GLUT1 played important role in the cancer cell-selective killing of **8a**, which provides new evidence for the targeted anticancer drug development based on GLUT1. **8a** had superior performance on the A549 3D tumor spheroids, that is, it could potently penetrate into and suppress the growth of tumor spheroids. Furthermore, because of the optimized properties of **8a**, intraperitoneal injection of **8a** demonstrated good therapeutic effect on A549 tumor models of mice without evident side effects, which provides direct evidence confirming the potential application of **8a** in anticancer drug development. In addition, our study established the relationship between cytotoxic activity and physiochemical

properties of monosaccharide-conjugated R-lycosin-I, which provides references for ACP optimization by glycosylation modification.

Experimental Section

General Experimental Procedure. Chemicals used were reagent grade as supplied except where noted. Analytical thin-layer chromatography was performed using silica gel 60 HF254 glass plates; Compound spots were visualized by UV light (254 nm), or in some cases by staining with a yellow solution containing ninhydrin (1.5 g) in butanol (100 mL)-HAc (3 mL), or by charring with 30% sulfuric acid-alcohol, or by staining with iodine in silica gel. Flash column chromatography was performed on columns (16×240 mm, 18×300 mm, 35×400 mm) of silica gel 60 (200-300 Mesh) with EtOAc-petroleum ether (60-90°C) as the eluent. Solutions were concentrated at <60°C under reduced pressure. NMR spectra were referenced using Me_4Si (0 ppm), residual $CHCl_3$ (^{1}H-NMR 7.26 ppm, ^{13}C NMR 77.3 ppm) for $CDCl_3$, using residual DOH (^{1}H-NMR 4.79 ppm) for D_2O, or using residual CD_3OH (^{1}H-NMR 4.87 ppm, ^{13}C NMR 49.0 ppm) for CD_3OD. Peak assignments are based on ^{1}H NMR, and ^{13}C NMR experiments. NMR experiments were conducted at 500, and 125 MHz for ^{1}H, ^{13}C, respectively, using Bruker Avance 500 MHz NMR Spectrometer equipped with a switchable QNP (^{1}H,^{13}C) probe enabling back-to-back data acquisition for the different nuclei without the need to remove sample or tune the probe. The glycopeptides were purified using preparing RP-HPLC (Milford, MA, USA) (column, C18, 300 Å, 10 × 250 mm; Welch Materials, Inc.) and determined using MALDI-TOF MS. All glycopeptide analogues evaluated in the biological assays were greater than 95% pure based on the HPLC methods. Purity, **8a**: 96.4 %, **8b**: 95.1 %, **8c**: 95.0 %, **8d**: 96.2 %, **8e**: 95.4 %.

Synthesis of 1,2,3,4,6-penta-*O*-acetyl-α,β-D-glucopyranose (1a)

In a 500 mL round bottom flask, the acetic anhydride (200 mL) was cooled to 0^{o}C under stirring. Then perchloric acid (1.0 mL) was added dropwise. The glucose (50.0 g, 277.8 mmol) was added in partition under the temperature was not excess 20^{o}C. The reaction mixture was stirring until TLC (petroleum ether : ethyl acetate = 3 : 1) showed the starting material was disappeared, during which time the temperature was gradually raised to ambient temperature. DCM (200 mL) was added, and then washed with water and CH_2Cl_2 for three times. The organic

layer was collected, dried over anhydrous sodium sulfate, filtered and the filtrate was evaporated on a rotavapor to give crude **1a** (106.6 g, 273.1 mmol, 98.3%) as a brown yellow syrup.

Synthesis of 1,2,3,4,6-penta-*O*-acetyl-α,β-D-galactopyranose (1b)

In a 1L round bottom flask, the acetic anhydride (400 mL) was cooled to 0°C under stirring. Then perchloric acid (0.4 mL) was added dropwise. The galactose (100.0 g, 0.56 mol) was added in partition under the temperature was not excess 10°C. The reaction mixture was stirring until TLC (petroleum ether: ethyl acetate = 3 : 1) showed the starting material was disappeared, during which time the temperature was gradually raised to ambient temperature. DCM (200 mL) was added to it, and then washed with water and CH_2Cl_2 for three times. The organic layer was collected, dried over anhydrous sodium sulfate, filtered and the solvent from the filtrate was evaporated on a rotavapor to give crude product **1b** (199.5 g, 0.51 mol, 92% yield) as a brown yellow syrup.

Synthesis of 1,2,3,4,6-penta-*O*-acetyl-α,β-D-mannopyranose (1c)

In a 500 mL round bottom flask, the acetic anhydride (100 mL) was cooled to 0°C under stirring. Then perchloric acid (1.0 mL) was added dropwise. The mannose (25.0 g, 138.9 mmol) was added in partition under the temperature was not excess 20°C. The reaction mixture was stirring until TLC (petroleum ether : ethyl acetate = 3 : 1) showed the starting material was disappeared, during which time the temperature was gradually raised to ambient temperature. DCM (200 mL) was added to it, and then washed with water and CH_2Cl_2 for three times. The organic layer was collected, dried over anhydrous sodium sulfate, filtered and the filtrate was evaporated on a rotavapor to give crude product **1c** (43.5 g, 111.4 mmol, 80.3%) as a brown yellow syrup.

Synthesis of 1,2,3,4-tetra-*O*-acetyl-α,β-L-arabinopyranose (1d)

In a 500 mL round bottom flask, the acetic anhydride (100.0 mL) was cooled to 0°C under stirring. Then perchloric acid (0.2 mL) was added dropwise. The L-arabinose (25.0 g, 166.7 mmol) was added in partition under the temperature was not excess 20°C. The reaction mixture was stirring until TLC (petroleum ether : ethyl acetate = 1 : 1) showed the starting material was disappeared, during which time the temperature was gradually raised to ambient temperature. DCM (100.0 mL)

was added to it, and then washed with water and CH_2Cl_2 for three times. The organic layer was collected, dried over anhydrous sodium sulfate, filtered and the solvent from the filtrate was evaporated on a rotavapor to give crude product **1d** (50.0 g, 157.2 mmol, 94.3%).

2-Acetamido-1,3,4,6-tetra-O-acetyl-2-deoxy-D-glucopyranose (1e)

A solution of D-glucosamine hydrochloride (6.0 g, 27.8 mmol) in a mixture of anhydrous pyridine (60 mL) and acetic anhydride (30 mL) was stirred overnight at RT. The mixture was diluted with 200 mL of chloroform and washed successively with cold water, saturated sodium bicarbonate solution, and finally with water. Then the solvent was removed to give compound **1e** (7.8 g, 20.0 mmol, 72%) as a white solid.

Synthesis of 2,3,4,6-tetra-*O*-acetyl-α,β-D-glucopyranose (2a)

In a 1 L round bottom flask, piperazine (25.0 g, 293.6 mmol) was added to the solution of compound **1a** (104.5 g, 267.7 mmol) in tetrahydrofuran (300 mL). The reaction mixture was stirring until TLC (petroleum ether : ethyl acetate = 2 : 1) showed the starting material was almost disappeared, filtered and the filtrate was evaporated on a rotavapor. The residue was washed with water and CH_2Cl_2.The organic layer was collected, dried over anhydrous sodium sulfate, filtered and concentrated, then purified by silica gel column chromatography with petroleum ether : ethyl acetate = 3 : 1 as the eluent to give compound **2a** (75.7 g, 217.3 mmol, 81.2%)as a pale-yellow syrup.

Synthesis of 2,3,4,6-tetra-*O*-acetyl-α,β-D-galactopyranose (2b)

In a 1 L round bottom flask, piperazine (14.6 g, 171.5 mmol) was added to the solution of compound **1b** (60.0 g, 153.7 mmol) in tetrahydrofuran (150 mL). The reaction mixture was stirring until TLC (petroleum ether : ethyl acetate = 2 : 1) showed the starting material was almost disappeared. The mixture was filtered and the filtrate was evaporated on a rotavapor. The residue was dissolved with CH_2Cl_2 and washed with water. The organic layer was collected, dried over anhydrous sodium sulfate, filtered and concentrated, then purified by silica gel column chromatography with petroleum ether : ethyl acetate = 3 : 1 as the eluent to give compound **2b** (42.0 g, 120.6 mmol, 78.5%) as a pale-yellow syrup.

Synthesis of 2,3,4,6-tetra-*O*-acetyl-α,β-D-mannopyranose (2c)

In a 1.0 L round bottom flask, piperazine (12.9 g, 151.5 mmol) was added to the solution of compound **1c (**29.0 g, 74.3 mmol) in tetrahydrofuran (150 mL). The reaction mixture was stirring until TLC (petroleum ether: ethyl acetate = 2: 1) showed the starting material was almost disappeared, filtered and the filtrate was evaporated on a rotavapor. The residue was washed with water and CH_2Cl_2. The organic layer was collected, dried over anhydrous sodium sulfate, filtered and concentrated, then purified by silica gel column chromatography with petroleum ether : ethyl acetate = 3 : 1 as the eluent to give compound **2c** (21.0 g, 60.3 mmol, 81.1%)as a pale-yellow syrup.

Synthesis of 2,3,4-tri-O-acetyl-α,β-L-arabinopyranose (2d)

In a 1000mL round bottom flask, piperazine (14.9 g, 172.8 mmol) was added to the solution of compound **1d** (50.0 g, 157.2 mmol) in tetrahydrofuran (100 mL). The reaction mixture was stirring until TLC (petroleum ether : ethyl acetate = 2 : 1) showed the starting material was almost disappeared, filtered and the filtrate was evaporated on a rotavapor. The residue was washed with water and CH_2Cl_2.The organic layer was collected, dried over anhydrous sodium sulfate, filtered and concentrated, then purified by silica gel column chromatography with petroleum ether : ethyl acetate = 3 : 2 as the eluent to give compound **2d** (20.8 g, 75.3 mmol, 47.9%).

2-Acetamido-3,4,6-tri-O-acetyl-2-deoxy-D-glucopyranose (2e)

To a stirred solution of **1e** (3.0 g, 7.7 mmol) in dry methanol (10 mL) and THF (40 mL) were introduced ammonia gas. The reaction mixture was stirred for 40 min at RT. The mixture was concentrated in vacuo and the residue was purified by flash column chromatography on silica gel (ethyl acetate : petroleum ether = 1 : 1) to give compound **2e** (1.75 g, 5.0 mmol, 65.2%) as a colorless oil.

Synthesis of 2,3,4,6-tetra-*O*-acetyl-α-D-glucopyranosetrichloroacetimine (3a)

In a 1 L round bottom flask, trichloroacetonitrile (58.4 mL, 582.4mmol) was added to a mixture of the intermediate **2a** (74.3 g, 213.3 mmol), K_2CO_3 (53.6 g, 388.4 mmol) in anhydrous DCM (400 mL). The mixture was stirring at room temperature until TLC (petroleum ether : ethyl acetate = 2 : 1) showed the starting material was almost disappeared, filtered and the solvent from the filtrate was evaporated on a rotavapor. The residue was purified by silica gel column chromatography with petroleum ether : ethyl acetate = 3 : 1 as the eluent to give compound **3a**

(80.0 g, 162.4 mmol, 76.1%) as a white solid.

Synthesis of 2,3,4,6-tetra-*O*-acetyl-α-D-galactopyranoyltrichloroacetimidate (3b)

In a 500 mL round bottom flask, trichloroacetonitrile (43 mL, 428.8 mmol) was added to a mixture of the intermediate **2b** (33.1 g, 95.0 mmol), K_2CO_3 (30.5 g, 220.3 mmol) in anhydrous DCM (400 mL). The mixture was stirring at room temperature until TLC (petroleum ether : ethyl acetate = 2 : 1) showed the starting material was almost disappeared, filtered and the filtrate was evaporated on a rotavapor. The residues were purified by silica gel column chromatography with petroleum ether : ethyl acetate = 3 : 1 as the eluent to give compound **3b** (40.3 g, 81.8 mmol, 96.1%) as a white solid.

Synthesis of 2,3,4,6-tetra-*O*-acetyl-α-D-mannopyranosyltrichloroacetimine (3c)

In a 250 mL round bottom flask, trichloroacetonitrile (22.6 mL, 120.0 mmol) was added to a mixture of the intermediate **2c (**20.0 g, 57.4 mmol), K_2CO_3 (25.0 g, 180.9 mmol) in anhydrous DCM (200 mL). The mixture was stirring at room temperature until TLC (petroleum ether : ethyl acetate = 2 : 1) showed the starting material was almost disappeared, filtered and the solvent from the filtrate was evaporated on a rotavapor. The residue was purified by silica gel column chromatography with petroleum ether : ethyl acetate = 3 : 1 as the eluent to give compound **3c** (24.7 g, 50.1 mmol, 87.3 %) as a white solid.

Synthesis of 2,3,4-tri-O-acetyl-β-L-arabinopyranosyltrichloroacetimidate (3d)

In a 500 mL round bottom flask, trichloroacetonitrile (22.5 mL, 225.5 mmol) was added to a mixture of the intermediate **2d** (20.0 g, 72.4 mmol), K_2CO_3 (20.8 g, 150.7 mmol) in anhydrous DCM (150 mL). The mixture was stirring at room temperature until TLC (petroleum ether : ethyl acetate = 2 : 1) showed the starting material was almost disappeared, filtered and the solvent from the filtrate was evaporated on a rotavapor. These residues were purified by silica gel column chromatography with petroleum ether : ethyl acetate = 4 : 1 as the eluent to give compound **3d** (19.7 g, 45.3 mmol, 62.5%).

2-Acetamido-3,4,6-tri-O-acetyl-2-deoxy-α-D-glucopyranosyl trichloroacetimidate (3e)

To a stirred solution of **2e** (1.2 g, 3.5 mmol) in dry dichloromethane (25 mL) were added trichloroacetonitrile (1.36 mL, 7.2 mmol) and anhydrous potassium carbonate (2.5 g, 18.1 mmol).

The reaction mixture was stirred for 3 h at RT. The crude product was filtered, concentrated and purified by flash column chromatography on silica gel (ethyl acetate : petroleum ether = 1 : 1) to give **3e** (1.1 g, 2.3 mmol, 67.5%) as a light yellow solid.

Synthesis of 3'-chloropropyl 2,3,4,6-tetra-*O*-acetyl-*β*-D-glucopyranoside (4a)

The compound **3a** (41.0 g, 83.2 mmol) and 4Å MS (3.0 g) were dried under vacuum for 2 h, then 3-chloro-1-propanol (25.0 mL, 179.4 mmol) and dry DCM (150 mL) were added. The mixture was stirred and cooled to -20°C, and then TMSOTf (260.0 μL, 1.5 mmol) was added under nitrogen atmosphere. The reaction mixture was stirring until TLC (petroleum ether: ethyl acetate = 3 : 1) showed the starting material was disappeared, during which time the temperature was gradually raised to ambient temperature. The mixture was washed with water and CH_2Cl_2. The organic layer was collected, dried over anhydrous sodium sulfate, filtered and the filtrate was evaporated on a rotavapor. The residue was purified by silica gel column chromatography with petroleum ether : ethyl acetate = 4 : 1 as the eluent to give compound **4a** (28.4 g, 66.8 mmol, 80.3%)as a pale-yellow syrup.

Synthesis of 3'-chloropropyl 2,3,4,6-tetra-*O*-acetyl-*β*-D-galactopyranoside (4b)

The compound **3b** (38.3 g,77.7 mmol) and 4Å MS (3.0 g) were dried under vacuum for 2 h, then 3-chloro-1-propanol (19.5 mL, 233.4 mmol) and dry DCM (150 mL) were added. The mixture was stirred and cooled to -20°C, and then TMSOTf (296.1 μL, 1.6 mmol) was added under nitrogen atmosphere. The reaction mixture was stirring until TLC (petroleum ether: ethyl acetate = 3 : 1) showed the starting material was disappeared, during which time the temperature was gradually raised to ambient temperature. The mixture was washed with water and CH_2Cl_2.The organic layer was collected, dried over anhydrous sodium sulfate, filtered and the filtrate was evaporated on a rotavapor. The residues was purified by silica gel column chromatography with petroleum ether: ethyl acetate = 4 : 1 as the eluent to give compound **4b** (29.1 g, 68.5 mmol, 88.2%) as a pale yellow syrup.

Synthesis of 3'-chloropropyl 2,3,4,6-tetra-*O*-acetyl-*α*-D-mannopyranoside (4c)

The compound **3c** (23.1 g, 46.9 mmol) and 4Å MS (3.0 g) were dried under vacuum for 2 h, then 3-chloro-1-propanol (8.5 mL, 101.7 mmol) and dry DCM (250 mL) were added. The mixture

was stirred and cooled to -20°C, and then TMSOTf (100.0 μL) was added under nitrogen atmosphere. The reaction mixture was stirring until TLC (petroleum ether : ethyl acetate = 3 : 1) showed the starting material was disappeared, during which time the temperature was gradually raised to ambient temperature. The mixture was washed with water and CH_2Cl_2. The organic layer was collected, dried over anhydrous sodium sulfate, filtered and the filtrate was evaporated on a rotavapor. The residue was purified by silica gel column chromatography with petroleum ether : ethyl acetate = 4 : 1 as the eluent to give compound **4c** (13.4 g, 31.5 mmol, 67.1%) as a pale-yellow syrup.

Synthesis of 3'-Chloropropyl 2,3,4-tri-O-acetyl-α-L-arabinopyranoside (4d)

The compound **3d** (19.0 g, 45.2 mmol) and 4Å MS (3 g) were dried under vacuum for 2 h, then 3-chloro-1-propanol (11.0 mL, 131.6 mmol) and dry DCM (200 mL) were added. The mixture was stirred and cooled to -20°C, and then TMSOTf (220.0 μL, 0.8 mmol) was added under nitrogen atmosphere. The reaction mixture was stirring until TLC (petroleum ether: ethyl acetate = 3 : 1) showed the starting material was disappeared, during which time the temperature was gradually raised to ambient temperature. The mixture was washed with water and CH_2Cl_2.The organic layer was collected, dried over anhydrous sodium sulfate, filtered and the solvent from the filtrate was evaporated on a rotavapor. These residues were purified by silica gel column chromatography with petroleum ether : ethyl acetate = 4 : 1 as the eluent to give compound **4d** (11.0 g, 31.1 mmol, 68.8%).

3'-Chloropropyl3,4,6-tri-O-acetyl-2-deoxy-2-acetamido-β-D-glucopyranoside (4e)

To a stirred solution of 3-chloropropanol (1.8 mL, 20.2 mmol) and **3e** (3.3 g, 6.71 mmol) in dichloromethane (30 mL) containing freshly activated 4 AMS (0.5 g) was slowly added TMSOTf (75 μL, 410.0 μmol) at -20°C. The reaction mixture was stirred for 30 min at RT. The crude product was filtered. After removal of solvent, the residue was purified by flash column chromatography on silica gel (ethyl acetate : petroleum ether = 1 : 2 to 1 : 1) to give compound **4e** (1.2 g, 2.8 mmol, 42.1%) as a white solid.

Synthesis of 3'-Azidopropyl 2,3,4,6-tetra-*O*-acetyl-β-D-glucopyranoside (5a)

Sodium azide (8.5 g, 130.8 mmol) was added slowly to a stirred solution of compound **4a** (27.6 g, 64.0 mmol) in DMF (150 mL). The reaction mixture was stirring at 75°C for 12 h until

TLC (petroleum ether: ethyl acetate = 2: 1) showed the starting material was disappeared. The mixture was washed with water and CH_2Cl_2. The organic layer was collected, dried over anhydrous magnesium sulfate, filtered and the filtrate was evaporated on a rotavapor. The residue was purified by silica gel column chromatography with petroleum ether : ethyl acetate = 3 : 1 as the eluent to give compound **5a** (21.8 g, 50.5 mmol, 78.9%) as a colorless syrup.

Synthesis of 3'-azidopropyl 2,3,4-tri-*O*-acetyl-β-D-galactopyranoside (5b)

Sodium azide (17.8 g, 273.9 mmol) was added slowly to a stirred solution of compound **4b** (28.5 g, 67.1 mmol) in DMF (150 mL). The reaction mixture was stirring at 75°C for 12 h until TLC (petroleum ether : ethyl acetate = 2 : 1) showed the starting material was disappeared. The mixture was washed with water and CH_2Cl_2. The organic layer was collected, dried over anhydrous magnesium sulfate, filtered and the filtrate was concentrated. The residues was purified by silica gel column chromatography with petroleum ether : ethyl acetate = 3 : 1 as the eluent to give compound **5b** (27.5 g, 63.7 mmol, 92.5%) as a colorless syrup.

Synthesis of 3'-azidopropyl 2,3,4,6-tetra-*O*-acetyl-α-D-mannopyranoside (5c)

Sodium azide (15.8 g, 243.1 mmol) was added slowly to a stirred solution of compound **4c** (12.6 g, 29.7 mmol) in DMF (150 mL). The reaction mixture was stirring at 75°C for 12 h until TLC (petroleum ether : ethyl acetate = 2 : 1) showed the starting material was disappeared. The mixture was washed with water and CH_2Cl_2. The organic layer was collected, dried over anhydrous magnesium sulfate, filtered and the filtrate was evaporated on a rotavapor. The residue was purified by silica gel column chromatography with petroleum ether : ethyl acetate = 3 : 1 as the eluent to give compound **5c** (8.1g, 18.8 mmol, 63.3%) as a colorless syrup.

Synthesis of 3'-Azidopropyl 2,3,4-tri-O-acetyl-α-L-arabinopyranoside (5d)

Sodium azide (11.1 g, 170.1 mmol) was added slowly to a stirred solution of compound **4d** (10.5 g, 29.8 mmol) in DMF (100 mL). The reaction mixture was stirring at 75°C for 12 h until TLC (petroleum ether : ethyl acetate = 2 : 1) showed the starting material was disappeared. The mixture was washed with water and CH_2Cl_2. The organic layer was collected, dried over anhydrous magnesium sulfate, filtered and the filtrate was evaporated on a rotavapor. These residue was purified by silica gel column chromatography with petroleum ether : ethyl acetate = 3 : 1 as the

eluent to give compound **5d** (10.7 g, 60.2%).

3'-Azidopropyl 2-acetamido-3,4,6-tri-O-acetyl-2-deoxy-β-D-glucopyranoside (5e)

To a solution of **4e** (200.0 mg, 471.9 μmol) in dry DMF (3 mL) were added NaN_3 (180.0 mg, 2.8mmol) and 18-crown-6 (50 mg). After stirring overnight at 60°C, the reaction mixture was diluted with ethyl acetate (150 mL), washed with brine, dried over Na_2SO_4, filtered and purified by flash column chromatography on silica gel (ethyl acetate : petroleum ether = 1 : 1) to give compound **5e** (165.7 mg, 385.1 μmol, 81.6%) as a white solid.

Synthesis of 3'-Azidopropyl β-D-glucopyranoside (6a)

Ammonia was bubbled to the solution of compound **5a** (20.0 g, 46.4 mmol) in methanol (150 mL). The reaction mixture was stirring until TLC (ethyl acetate : methanol = 3 : 1) showed the starting material was disappeared. Then the mixture was concentrated and the residue was purified by silica gel column chromatography with ethyl acetate: methanol = 5 : 1 as the eluent to give compound **6a** (10.5 g, 40.1 mmol, 86.4%) as a pale-yellow syrup.

Synthesis of 3'-azidopropyl β-D-galactopyranoside (6b)

Ammonia was bubbled to the solution of compound **5b** (26.4 g, 61.2 mmol) in methanol (150 mL). The reaction mixture was stirring until TLC (ethyl acetate : methanol = 3 : 1) showed the starting material was disappeared. Then the mixture was concentrated and the residue was purified by silica gel column chromatography with ethyl acetate: methanol = 5 : 1 as the eluent to give compound **6b** (15.3 g, 58.1 mmol, 95.0%) as a pale-yellow syrup.

Synthesis of 3'-azidopropyl α-D-mannopyranoside (6c)

Ammonia was bubbled to the solution of compound **5c** (15.6 g, 36.2 mmol) in methanol (150 mL). The reaction mixture was stirring until TLC (ethyl acetate : methanol = 3 : 1) showed the starting material was disappeared. Then the mixture was concentrated and the residue was purified by silica gel column chromatography with ethyl acetate : methanol = 5 : 1 as the eluent to give compound **6c** (7.0 g, 26.6 mmol, 73.4%) as a pale-yellow syrup.

Synthesis of 3'-Azidopropyl α-L-arabinopyranoside (6d)

Ammonia was bubbled to the solution of compound **5d** (9.2 g, 25.6 mmol) in methanol (150 mL).

The reaction mixture was stirring until TLC (ethyl acetate : methanol = 3 : 1) showed the starting material was disappeared. Then the mixture was concentrated and the residue was purified by silica gel column chromatography with ethyl acetate : methanol = 10 : 1 as the eluent to give compound **6d** (3.4 g, 57.6%).

3'-Azidopropyl 2-deoxy-2-acetamido-β-D-glucopyranoside (6e)

To a stirred solution of **5e** (2.2 g, 4.7 mmol) in dry methanol (15 mL) were introduced ammonia gas. The reaction mixture was stirred for overnight at RT. After removal of solvent, the residue was purified by flash column chromatography on silica gel (ethyl acetate : methanol = 4 : 1) to give compound **6e** as a white solid (1.4 g, 4.5 mmol, 96.7%).^{1}H NMR (500 MHz, MeOD): δ (ppm) 4.39 (d, 1 H, $J_{1,2}$ = 8.5 Hz, H-1), 3.98-3.94 (m, 1 H, $OCH_2CH_2CHHN_3$), 3.89 (dd, 1 H, $J_{6a,5}$ = 12.0 Hz, $J_{6a,6b}$ = 2.0 Hz, H-6a), 3.70 (dd, 1 H, $J_{6b,5}$ = 5.5 Hz, $J_{6b,6a}$ = 2.0 Hz, H-6b), 3.65 (dd, 1 H, $J_{3,2} = J_{3,4}$ = 8.5 Hz, H-3), 3.56 (ddd, 1 H, $J_{5,4}$ = 8.5 Hz, $J_{5,6a}$ = 12.0 Hz, $J_{5,6b}$ = 5.5 Hz, H-5), 3.88 (d, 1 H, $J_{4,3} = J_{4,5}$ =8.5 Hz, H-4), 3.40-3.26 (m, 5 H, H-2, NHAc, $OCH_2CH_2CHHN_3$, $OCH_2CH_2CH_2N_3$), 1.99 (s, 3 H, $NHCOCH_3$), 1.83-1.79 (m, 2 H, $OCH_2CH_2CH_2N_3$); ^{13}CNMR(125 MHz, MeOD): δ (ppm) 173.7 (1 C, CH_3CO), 102.8 (1 C, C-1), 77.9 (1C,C-3), 75.9 (1C,C-2), 72.1 (1C,C-5), 67.1 (1C,C-4), 62.8 (1C,$OCH_2CH_2CH_2Cl$), 57.3 (1C,C-6), 48.4 (1 C, $OCH_2CH_2CH_2N_3$), 30.0 (1 C, $OCH_2CH_2CH_2N_3$), 23.0 (1 C, $NHCOCH_3$).

Synthesis of 3'-aminopropyl β-D-glucopyranoside (7a)

In a 500 mL round bottom flask, PPh_3 (11.9 g, 45.3 mmol) was added to the solution of compound **6a** (10.0 g, 38.0 mmol) in THF (200 mL) and H_2O (40 mL) under stirring. The reaction mixture was refluxed at 75°C until TLC (ethyl acetate : methanol = 2 : 1) showed the starting material was disappeared. The mixture was concentrated and a white solid was precipitated after water (20 mL) was dropwise added. The mixture was filtered, the filtrate was evaporated to dryness and dried by vacuum to give yellowish syrup **7a** (4.8 g, 20.3 mmol, 53.4%). ^{1}H NMR (500 MHz, D_2O): δ (ppm) 4.34 (d, 1H, $J_{1,2}$ = 7.9 Hz, H-1), 4.95-3.87 (m, 2H, H-2, H-3), 3.73-3.44 (m, 6H, H-4, H-5, H-6a, H-6b, $OCH_2CH_2CH_2NH_2$), 2.78-2.76 (t, 2H, J = 7.0 Hz $OCH_2CH_2CH_2NH_2$), 1.77-1.73 (m, 2H, $OCH_2CH_2CH_2NH_2$); ^{13}C NMR (125 MHz, D_2O): δ (ppm): 102.7 (1C, C-1), 75.1 (1C, C-2), 72.7 (1C, C-3), 70.7 (1C, C-4), 68.6 (1C, C-5), 68.2 (1C, $OCH_2CH_2CH_2NH_2$), 60.9 (1C, C-6), 37.5 (1C, $OCH_2CH_2CH_2NH_2$), 30.4 (1C, $OCH_2CH_2CH_2NH_2$).

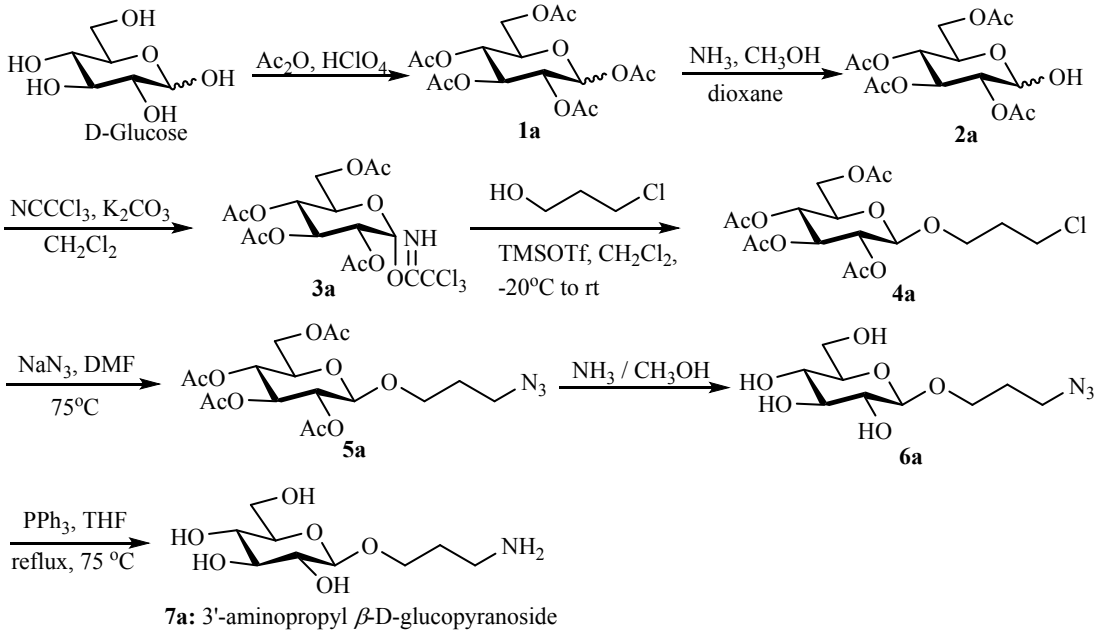

Scheme 1 Synthesis of 3'-aminopropyl-D-glucopyranoside (**7a**).

Synthesis of 3'-aminopropylβ-D-galactopyranoside (7b)

In a 500 mL round bottom flask, PPh_3 (23.2 g, 88.3 mmol) was added to the solution of compound **6b** (15.0 g, 57.0 mmol) in THF (200 mL) and H_2O (40 mL) under stirring. The reaction mixture was refluxed at 75°C, until TLC (ethyl acetate: methanol = 2 : 1) showed the starting material was disappeared. The mixture was concentrated and a white solid was precipitated after water (20 mL) was added dropwise. The mixture was filtered, and the filtrate was evaporated to dryness and dried by vacuum to give yellowish syrup **7a** (10.8 g, 45.5 mmol, 79.8%). ^{1}H NMR (500 MHz, D_2O): δ (ppm) 4.41 (d, 1H, $J_{1,2}$ = 7.6 Hz, H-1), 4.03-3.93 (m, 2H, H-2, H-3), 3.79-3.72 (m, 2H, H-4, H-5), 3.70 (dd, 1H, $J_{6a,5}$ = 8.8, $J_{6a,6b}$ = 5.0 Hz, H-6a), 3.69 (dd, 1H, $J_{6b,5}$ = 8.6 Hz, $J_{6b,6a}$ = 6.3 Hz, H-6b), 3.57-3.53 (m, 2H, $OCH_2CH_2CH_2NH_2$), 2.85-2.82 (t, 2H, J = 7.0 Hz $OCH_2CH_2CH_2NH_2$), 1.85-1.82 (m, 2H, $OCH_2CH_2CH_2NH_2$); ^{13}C NMR (125 MHz, D_2O): δ (ppm): 102.8 (1C, C-1), 75.1 (1C, C-2), 72.7 (1C, C-3), 70.7 (1C, C-4), 68.6 (1C, C-5), 68.2 (1C, $OCH_2CH_2CH_2NH_2$), 60.9 (1C, C-6), 37.5 (1C, $OCH_2CH_2CH_2NH_2$), 30.2 (1C, $OCH_2CH_2CH_2NH_2$).

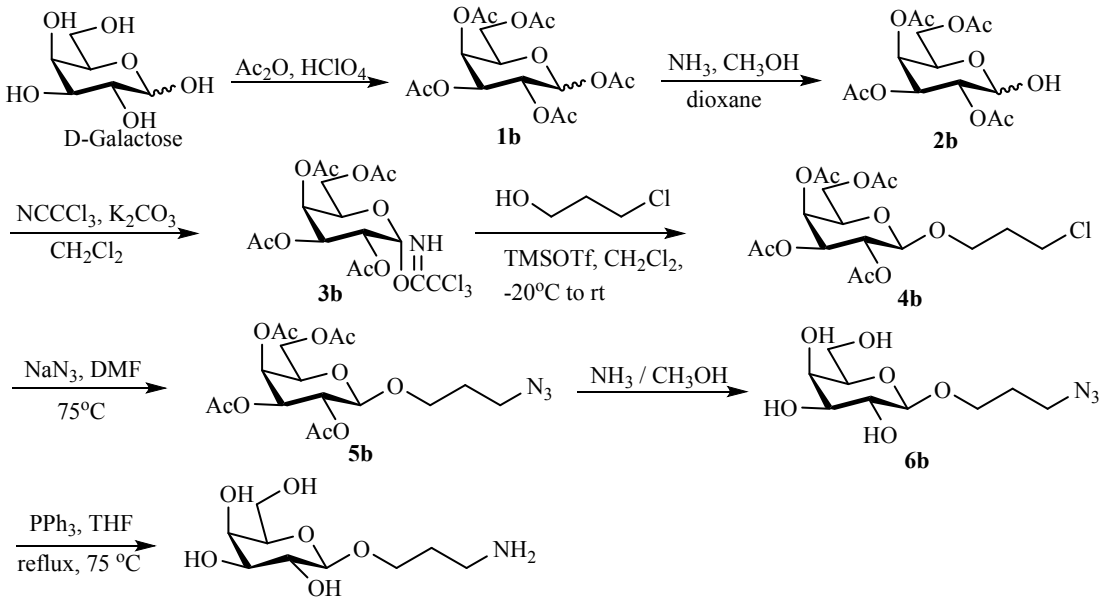

Scheme 2 Synthesis of 3'-aminopropyl β-D-galactopyranoside (**7b**)

Synthesis of 3'-aminopropyl-α-D-mannopyranoside (7c)

In a 100 mL round bottom flask, PPh_3 (11.7 g, 44.3 mmol) was added to the solution of compound **6c** (6.5 g, 24.7 mmol) in THF (100 mL) and H_2O (20 mL) under stirring. The reaction mixture was refluxed at 75°C, until TLC (ethyl acetate : methanol = 2 : 1) showed the starting material was disappeared. The mixture was concentrated and a white solid was precipitated after water (10 mL) was added dropwise. The mixture was filtered, the filtrate was evaporated to dryness and dried by vacuum to give yellowish syrup **7c** (4.3 g, 18.2 mmol, 73.9%). ^{1}H NMR (500 MHz, D_2O): δ (ppm) 4.82 (d, 1H, $J_{1,2}$ = 3.5 Hz, H-1), 3.96-3.52 (m, 8H, H-2, H-3, H-4, H-5, H-6a, H-6b, OCH_2CH$_2$CH$_2$NH$_2$), 3.07-3.00 (m, 2H, OCH$_2$CH$_2$CH_2NH$_2$), 1.96-1.87 (m, 2H, OCH$_2$CH_2CH$_2$NH$_2$); ^{13}C NMR (125 MHz, D_2O): δ (ppm): 99.7 (1C, C-1), 72.8 (1C, C-5), 70.5(1C, C-3), 69.9 (1C, C-2), 66.7 (1C, C-4), 65.1(1C, O*C*H$_2$CH$_2$CH$_2$NH$_2$), 60.9 (1C, C-6), 37.5 (1C, OCH$_2$CH$_2$*C*H$_2$NH$_2$), 27.7 (1C, OCH$_2$*C*H$_2$CH$_2$NH$_2$).

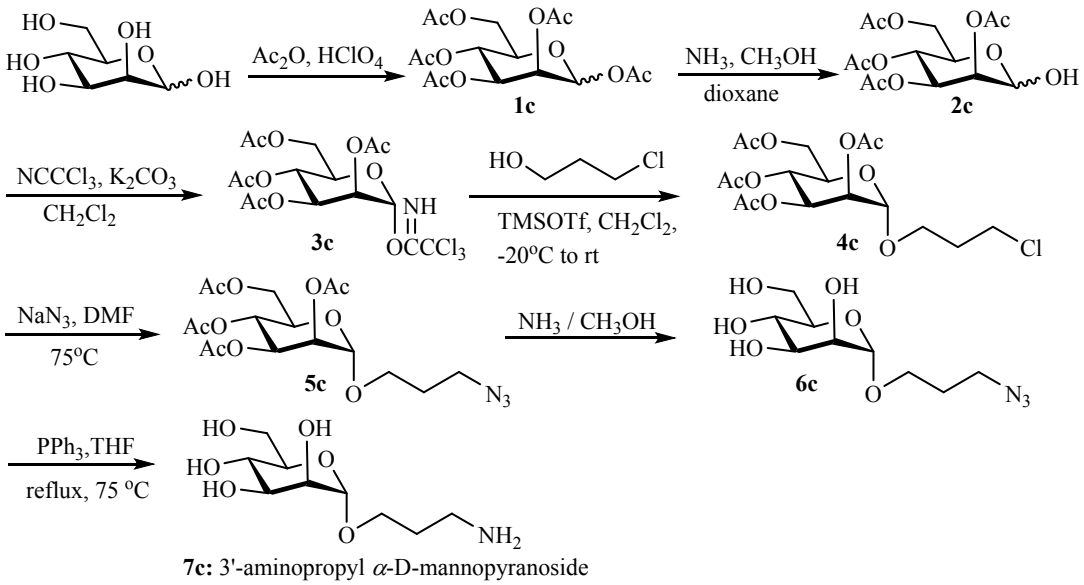

Scheme 3 Synthesis of 3'-aminopropyl α-D-mannopyranoside (**7c**)

Synthesis of 3'-aminopropyl α-L-arabinopyranoside (7d)

In a 100 mL round bottom flask, PPh_3 (5.7 g, 21.8 mmol) was added to the solution of compound **6d** (3.4 g, 14.6 mmol) in THF (40.0 mL) and H_2O (8.0 mL) under stirring. The reaction mixture was refluxed at 75°C, until TLC (ethyl acetate : methanol = 2 : 1) showed the starting material was disappeared. The mixture was concentrated and a white solid was precipitated after water (2.0 mL) was added dropwise. The mixture was filtered, then the mother liquor was evaporated to dryness and dried by vacuum to give yellowish syrup **7d** (2.3 g, 72.3 %). ^{1}H NMR (500 MHz, D_2O): δ (ppm) 4.37 (t, 1H, $J_{1,2}$=7.5 Hz, H-1), 4.01-3.91 (m, 3H, H-2, H-3, H-4), 3.69-3.53 (m, 4H, 2 H-5, OCH_2CH$_2$CH$_2$NH$_2$), 3.09-3.03 (t, 2H, J = 6.7Hz, OCH$_2$CH$_2$CH_2NH$_2$), 1.95 (m, 2H, OCH$_2$CH_2CH$_2$NH$_2$); ^{13}C NMR (125 MHz, D_2O): δ 103.0 (1C, C-1), 72.3 (1C, C-3), 70.7 (1C, C-2), 68.2 (1C, C-4), 67.9 (1C, C-5), 66.2 (1C, OCH$_2$CH$_2$CH$_2$NH$_2$), 37.8 (1C, OCH$_2$CH$_2$$CH_2NH_2$), 27.4 (1C, OCH$_2$$CH_2CH_2NH_2$).

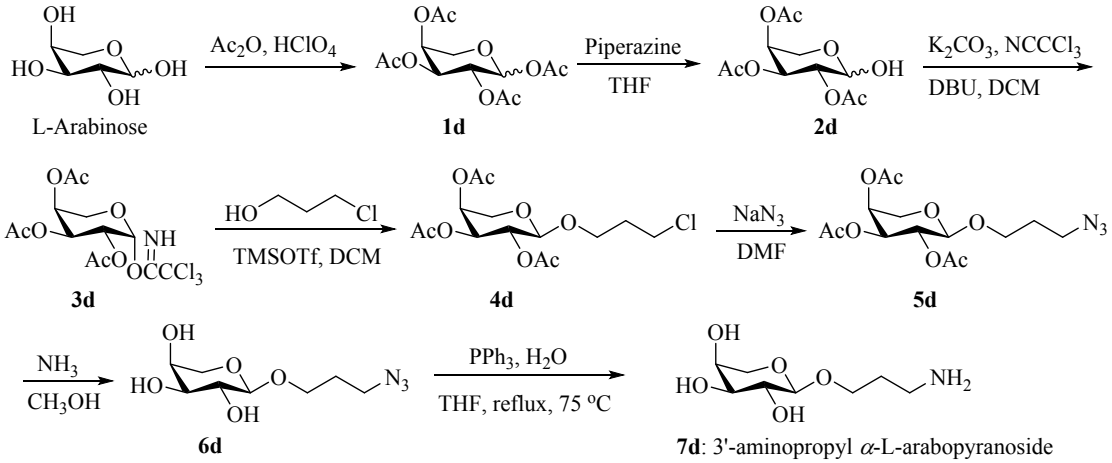

Scheme 4 Synthesis of 3'-aminopropyl α-L-arabinopyranoside (**7d**)

3'-Aminopropyl 2-deoxy-2-acetamido-β-D-glucopyranoside (7e)

In a 50 mL round bottom flask, a mixture of the azide intermediate **6e** (1.0 g, 3.3 mmol) and triphenyl phosphine (1.1 g, 3.9 mmol) dissolved in tetrahydrofuran (15 mL) was stirred at room temperature. After 10 min, water (3.0 mL) were added and the reaction mixture was kept under stirring for 4h at 70°C.The reaction mixture was concentrated on rotary evaporator and then added water. The white solid was precipitated in the flask. The white solid was filtered. After removal of solvent, the residue was dried under vacuum to give compound **7e** as syrup (797.2 mg, 2.9 mmol, 86.8%).^{1}H NMR (500 MHz, D_2O): δ (ppm) 4.60 (d, 1 H, $J_{1,2}$ = 8.5 Hz, H-1), 4.12-4.08 (m, 1 H, N*H*COCH$_3$), 4.03-3.50 (m, 9 H, H-6a, H-6b, H-3, H-5, H-4, H-2, OCH$_2$CH$_2$C*H*$_2$NH$_2$, OC*H*$_2$CH$_2$CH$_2$NH$_2$), 2.15 (s, 3 H, NHCOC*H*$_3$), 2.03-1.99 (m, 2 H, OCH$_2$C*H*$_2$CH$_2$NH$_2$); ^{13}CNMR(125 MHz, D_2O): δ (ppm) 174.7 (1 C, CH$_3$*C*O), 101.1 (1 C, C-1), 75.9, 73.6, 70.0, 67.9, 60.7 (5C,C-2,C-3,C-4,C-5,C-6),55.5(1C,O*C*H$_2$CH$_2$CH$_2$NH$_2$), 37.6 (1 C, OCH$_2$CH$_2$*C*H$_2$NH$_2$), 27.5 (1 C, OCH$_2$*C*H$_2$CH$_2$NH$_2$), 22.2 (1 C, NHCO*C*H$_3$).

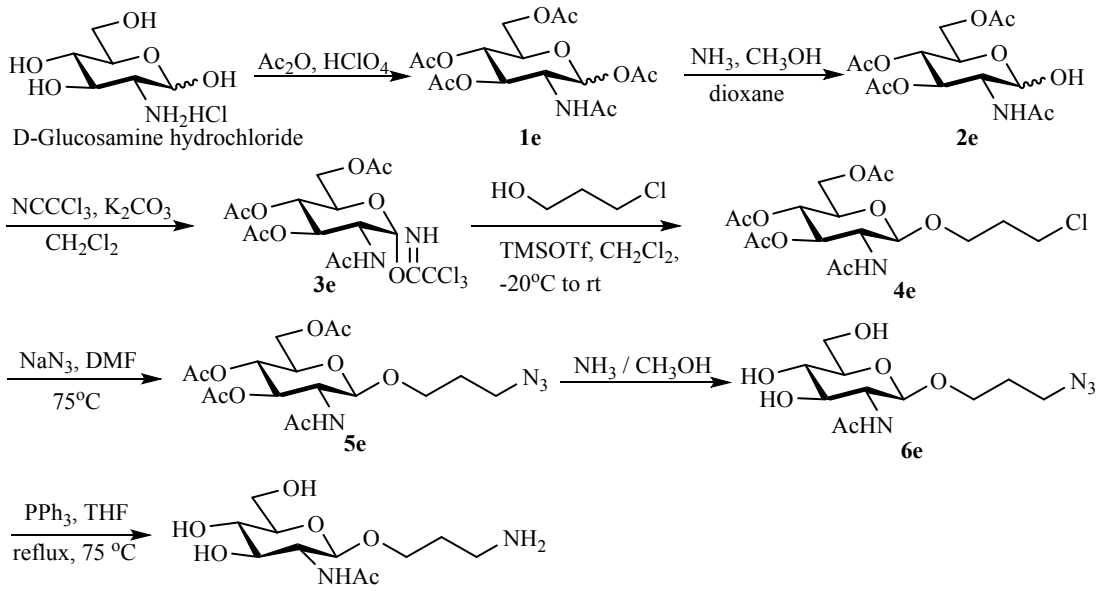

Scheme 5 Synthesis of 3'-aminopropyl 2-deoxy-2-acetamido-*β*-D-glucopyranoside (**7e**)

Glycopeptides synthesis, purification and determination

Monosaccharide derivatives **7a-e** were conjugated to the *N*-terminal of R-lycosin-I via the Glutaric anhydride linker. Dehydration condensation reaction occurs in HATU/HOBT *N*-methylmorpholine solution. By lysis, ether precipitation, air drying, crude glycopeptides were obtained. The synthetic glycopeptides were fractionated using preparing RP-HPLC (Milford, MA, USA) (column, C18, 300 Å, 10 × 250 mm; Welch Materials, Inc.) via a 0.1% TFA/acetonitrile gradient (0-80% for 48 min) at a flow rate of 3 mL/min. After collected corresponding glycopeptides peak, analytical C18 RP-HPLC analysis was performed to second purification at a flow rate of 1 mL/min. The purity was assessed at 280 nm. The eluted fractions were submitted for mass determination using MALDI-TOF MS. For AB Sciex-TOF/TOF 5800 mass spectrometer (Applied Biosystems, USA) analysis, a 1 μL aliquot of each glycopeptide elution was spotted onto a 96-well target plate along with an equal volume of a matrix solution containing 20 mg/mL α-cyano-4-hydroxycinnamic acid (CCA), 50% ACN, and 0.1% TFA. Mass spectrometry was performed at an acceleration voltage of 25 kV.

Cell cultures

Human lung carcinoma cells (A549, H460 and H1437), human prostatic carcinoma cell (PC-3), gastric cancer cell (HGC-27), human breast cell (MDA-MB-231) and non-cancer cells

(HEK-293T and L-02) were purchased from ATCC. A549-luciferase cells were purchased from Hanbio Biotechnology Co., Ltd. Cells were cultured in F12K medium (Gibco) or DMEM medium (Gibco) containing 100 U/mL penicillin, 100 mg/mL streptomycin, and 10% fetal bovine serum (FBS, Gibco) at 37 °C with 5% CO_2.

Dynamic light scattering and circular dichroism analysis

The hydrodynamic size and zeta-potential of compounds were characterized by dynamic light scattering (DLS, Zetasizer Nano ZSP, and Malvern, UK) at a concentration of 100 μM. The secondary structure was determined by circular dichroism (CD) spectroscopy. Measurements were performed in the UV range of 195-260 nm at a concentration of 100 μM at 25°C in PBS or 50% TFE using a Jasco-810 spectropolarimeter. The mean residue molar ellipticities were calculated using the equation $[\theta] = \theta/10lcMn$, where θ is the ellipticity in millidegrees, l is the optical path length of the cuvette in centimeters, cM is the peptide concentration in mole/liter, and n is the number of residues in the peptide.

Cell viability assay

Cells were seeded onto a 96-well plate at around 2×10^3 cells/well and incubated overnight. The cells were treated with fresh serum-free medium containing different concentration peptides for 24 h. After 24 h, CCK-8 were added to corresponding wells (10 μL CCK-8/well). The cell viability was determined using the Cell Counting Kit-8 which is purchased from Sellack.

Flow cytometry assay

A549 cells were seeded ($2\text{-}3 \times 10^5$ cells/well) in 6-well plates. After cells were cultured in 37°C, 5% CO_2 for 24 h, washed once with fresh PBS and trypsinized. the cells were re-suspended with medium containing 8 μM peptides and incubated for 4 h. After centrifuged three times, the cell pellet was lightly washed three times with cold PBS and then stained by Annexin-V-FITC/PI apoptotic detection kit according to the manufacturer's instructions. The fluorescence was measured using flow cytometry (BD, USA).

Colony formation assay

For examining the survival of cancer cells treated with R-lycosin-I and **8a**, cells were counted

and seeded into 6-well plate in a range of 300 cells per plate. After 36 h, cells were treated with 4 μM peptides which were refilled after 7 days. The cells were in total incubated for 15 days at 37°C in a humidified 5% CO_2 atmosphere. All the colonies were stained with 2% crystal violet.

Cellular localization analysis

A549 cells were seeded onto Glass Bottom Cell Culture Dish (Cat. No.: J40141) and incubated overnight. The cells were then incubated with fresh medium containing 15 μM FITC-R-lycosin-I and FITC-**8a** for 2 h. The cells were lightly washed thrice with fresh PBS. Mito-tracker-Red (100 nM) were added and incubated for 1 h. Then DAPI (diluted 1 : 1000) were added and incubated for another 15 min after being washed twice with fresh PBS and imaged using a laser confocal microscope (Olympus FV1000).

Cellular uptake

For the cellular uptake experiment, the A549 cells were seeded onto a 24-well plate at 1×10^5 cells per well and incubated overnight. The media were replaced with fresh media containing different concentrations of FITC-R-lycosin-I and FITC-**8a** which were incubated with the cells for 0.5 h, 1 h, and 2 h, respectively， followed by lightly washing 3 times with PBS and images were evaluated by Olympus fluorescent microscope. For quantitative analysis, the cells were washed once with fresh PBS and trypsinized. The cells were resuspended in fresh media and treated with same concentration and time as described by image evaluation. After A549 cells were treated with the FITC-labeled peptides fro corresponding time, the numbers of total and fluorescent cells were determined using cello-meter K2 (Nexcelom, USA), respectively.

Cytotoxic activity inhibition by STF-31 in A549 cells

A549 cells were seeded onto a 96-well plate at 2×10^3 cells/well and incubated overnight. The medium was aspirated, F12K (supplemented with 10% FBS and 1% penicillin/streptomycin) medium with or without STF-31 (1 μM final concentration, purchased from selleck.cn Cat. No. S7931) was added in corresponding wells, and the cells were incubated for 4 h. Then stock solutions (F12K medium supplemented with 1 μM STF-31) of peptides (R-lycosin-I, **8a** or **8b**) were added to afford a final concentration of 12.5 μM and the cells were incubated for additional 2 h at 37°C. The cell viability was determined using the Cell Counting Kit-8.

Immunoblotting analysis of GLUT1 protein

2×10^5 A549 or HEK-293T cells were seeded on 35 mm petri dishes and incubated for 24 h at 37°C. Cells were then washed 3 times with PBS, scraped into 2×SDS-PAGE loading buffer, and boiled at 100°C for 5 min. Whole cell lysates were resolved by 12% sodium dodecylsulfate polyacrylamide gel electrophoresis (SDS-PAGE; 100 V for 30 min and then 150 V for 1 h) followed by electro transfer to a polyvinylidene difluoride membrane, PVDF (200 mA for 1 h). Membranes were blocked using 5% (w/v) skim milk in TBST (PBS/0.1% Tween 20) and then incubated with GLUT1 (Proteintech, China. Catalog number: 66290-1-Ig) or GAPDH (Cell Signaling Technology) primary antibodies overnight at 4°C. On the following day, after washing 3 times with TBST, the membrane was incubated with secondary antibodies (Proteintech, China) in fresh BSA blocking solution. Immune complexes were detected with the ECL detection reagent (Beyotime, Shanghai, China. P0018AS).

Membrane integrity

A549 Cells were plated at a density of 2×10^3 cells/well in a 96-well plate and allowed to adhere overnight. R-lycosin-I and **8a** were then added to corresponding well with various concentrations and incubated for 2 h, respectively. LDH analysis was carried out according to the manufacturer's instructions of LDH Cytotoxicity Assay Kit [44] (Beyotime, Shanghai, China. C0017). The absorbance of each well was measured at 490 nm with Absorbance Microplate Reader (BioTek Instruments, USA)

Scanning electron microscope analysis

In order to examine cell morphological changes after drug treatment, A549 cells (2×10^3 cells/mL) were pre-seeded on the mica sheet under the bottom of the sterile 12-well plate for 24 h at 37°C. The cells were treated with R-lycosin-I and **8a** at the concentration of 15 μM for 24 h at 37°C, and then the cells were washed twice with PBS and fixed with 4% paraformaldehyde for 15 min. The fixed cells were dehydrated with a gradation of ethanol concentrations. Cells were observed using a JSM-840 scanning electron microscope operated at 15 kV.

Mitochondrial membrane potential analysis

To determine whether R-lycosin-I and **8a** could destroy mitochondrial membrane potentials (MMPs), JC-1 assay was performed according to the manufacturer's instructions of JC-1 kit (Beyotime, China). MMPs were monitored by determining the relative amounts of dual emissions from mitochondrial JC-1 monomers or aggregates using an Olympus fluorescent microscope. Mitochondrial depolarization is indicated by an increase of the green/red fluorescence intensity ratio.

Cytochrome C release determination

The cytochrome C (CytC) release was detected according to literature procedure[49]. Briefly, after treated A549 cells with 15 μM R-lycosin-I and **8a** for 24 h, cells were permeabilized (for 2 min) and then blocked (for 30 min) by 0.5% Triton X-100 and the blocking buffer (10% (v/v) sheep serum in PBS), respectively. After treating for the indicated time and washing with PBS, these cells were incubated with primary antibody of CytC (1 : 100) at RT for 2 hours, and after removing the unbound antibody, the fluorescence-labeled goat anti-mouse secondary antibody (1 : 200) was added and incubated for an additional 1 hour. After removing unbound secondary antibody with PBS, these cells were covered, fixed and then observed using the laser confocal microscope (Olympus FV1000). Note that the cells untreated by peptides were used as the control.

Caspase 3 activity assay

The activity of caspase 3 in A549 cells was assessed according to the manufacturer's instructions of Caspase 3 activity assay Kit (Beyotime, Shanghai, China, C1115). In brief, A549 cells were treated for 24 h with culture medium (as control) or 15 μM R-lycosin-I or **8a**. Then, the cells were harvested, lysed, and centrifugated. Supernatants were collected and incubated with Ac-DEVD-*p*NA (2mM) which is the substrate of caspase 3. The activity of caspase 3 was determined based on the absorbance at 405 nm by Absorbance Microplate Reader (BioTek Instruments, USA). The caspase 3 activity ratio was calculated as compared to the blank control.

Penetration and toxicity in tumor spheroids

A549 3D tumor spheroids were grown to study the penetration and toxicity of the peptides in a 3D tumor model. To determine the toxicity of the peptides on the 3D tumor model, the A549 spheroids were treated with the final concentration of 30 μM R-lycosin-I or **8a** for total 6 days in a

48 well plate and the peptides were refilled every 2 days. At the day 0, 200 μL 10% fresh culture medium containing 30 μM peptides were added to wells which contain one 3D tumor. At day 2 and day 4, the peptides (the final concentration of 30 μM) were added to corresponding wells and incubated for another 2 days. Subsequently, the spheroids were washed thrice with fresh medium and imaged using a microscope, and the cell viability was measured using the CCK-8 Assay. The tumor image evaluation and size measure were taken at day 0, day 3 and day6. For tumor spheroids penetration, the medium was replaced with fresh medium containing fluorescence-labeled R-lycosin-I or **8a** at 30 μM for 2 h. As for the confocal imaging, the spheroids were mounted on Glass Bottom Cell Culture Dish. The spheroids were imaged using a confocal microscope to obtain the Z-stack images, preceding every 8 μm until the laser penetration faltered.

Inhibition of tumor growth in human lung carcinoma xenografts

4 to 6 weeks-old healthy male BALB/c nu/nu mice were purchased from Slac & Jingda Corporation of laboratory animals, Changsha, China. All the animal studies were approved by the Institutional Animal Care and Use Committee (IACUC) of Hunan Normal University, and the National Institutes of Health guidelines for the performance of animal experiments were followed. 200 μL of 108/mL A549-luciferase cells suspended in sterile PBS buffer were subcutaneously injected into the right back of each mouse. When tumors reached the size of 100-200 mm^3, all mice were divided into 2 parts (one part includes 4 groups of five animals each). One part of mice was injected 200 μL of R-lycosin-I or **8a** (9 mg/kg) by intraperitoneal injection. Control group of mice was injected with isopyknic sterile PBS. Another part of mice was injected 100 μL of R-lycosin-I or **8a** (3 mg/kg) intratumorally and the injection of 100 μL PBS was also performed as negative control. Note that we defined the injection day as day 0. The injection was carried out every other day for 7 times in intraperitoneal injection part and every 3 days for 4 times in another part. According to the literature procedure[54], at day 14 in intraperitoneal injection part and 12 in another part, all A549-luciferase tumor bearing mice each group were received i.p. injection of 200 μL, 15 mg/mL D-luciferin (D-luciferin, firefly, potassium salt, SynChem, Inc.) and then anesthetized with 8% chloralhydrate. Ten minutes later, bioluminescent imaging of A549-luciferase tumor was performed using a multi-modal *in vivo* imaging system (Bruker In

Vivo FX Pro) according to the manufacturer's instructions. Additionally, the tumor size and body weight of mice in each group were also monitored. Tumor tissues and main organs (heart, liver and kidney) were fixed in 10% paraformaldehyde and dissected for histology observation. The tumor tissues were embedded in paraf, sectioned and stained by TUNEL assay. The main organs were stained by H&E assay.

Ancillary Information

Supporting Information: The Supporting Information is available free of charge on the ACS Publications website. Supporting Information Page 3-8 contains the ^{1}H NMR and ^{13}C NMR spectra of **7a**, **7b**, **7c**, **7d**, **7e**. **Figure S1** represents the analytical RP-HPLC and mass spectra of **8c**, **8d** and **8e**. **Figure S2** reports live cell statistics of trypan blue staining experiments. **Figure S3** indicates TEM images of the R-lycosin-I and glycopeptides. **Figure S4** shows effect of GLUT1 inhibitor STF-31 on the cytotoxic activity of **8d** and LDH leakage in A549 cells and HEK293T cells after treatment with **8a**, **8b** and **8d**. **Figure S5** reports SEM image evaluation of R-lycosin-I. **Figure S6** reports cell viability assay of the R-lycosin-I and **8a** against A549-luciferase cells. **Figure S7** represents serum stability of R-lycosin-I and glycopeptides. **Table S1** demonstrates oligos used for knockdown of GLUT1.

Molecular Formula Strings file is also available.

Author Information

Corresponding Author: *youlinzengcn@gmail.com and *liuzh@hunnu.edu.cn

Author Contribution: Peng Zhang and Jing Ma contributed equally to this work. All glycopeptides were synthesized, purified, and characterized by Jing Ma. Jing Ma also run some of bioactivity experiments. Peng Zhang organized and run most of the bioactivity experiments. Qianqian Zhang, Shandong Jian, Xiaoliang Sun, Bobo Liu, Liqin Nie and Meiyan Liu did some chemical synthesis work or bioactivity experiments. Peng Zhang, Songping Liang, Youlin Zeng and Zhonghua Liu designed the experiment and wrote the manuscript. All authors reviewed the manuscript.

Statistical Analysis

Statistical analyses were performed by using GraphPad Prism software version 5.0. Data were analyzed by using the One-way ANOVA test (and nonparametric). The levels of significance were assigned as *P ≤ 0.05, **P ≤ 0.01, and ***P ≤ 0.001.

Acknowledgments

This research was financially supported by the National Nature Sciences Foundation of China (General Program: 21877036, 31670783), the Science Fund for Distinguished Young Scholars of Hunan Province (no. 14JJ1018), the Opening Fund of The National &Local Joint Engineering Laboratory of Animal Peptide Drug Development (Hunan Normal University), National Development and Reform Commission (2017KF003), Science and Technology Planning Project of Hunan Province (2018TP1017) and the Cooperative Innovation Center of Engineering and New Products for Developmental Biology of Hunan Province (no. 20134486).

Abbreviations Used

GLUT1: Glucose transporter 1

ACPs: Anticancer peptides

SCLC: Small cell lung cancer

FITC: Fluorescein isothiocyanate

PDI: Polymer dispersity index

DLS: Dynamic light scattering

NE: Nuclear envelope

LDH: Lactate dehydrogenase

MMP: Mitochondrial membrane potential

Cyt-C: Cytochrome C

RT: Room temperature

CCA: α-cyano-4-hydroxycinnamic acid

CD: circular dichroism

CCK-8: Cell Counting Kit-8

References

1. Arteaga, C. L.; Baselga, J. Impact of genomics on personalized cancer medicine. *Clinical*

Cancer Research an Official Journal of the American Association for Cancer Research **2012,** 18, 612-618.

2. Jemal, A.; Siegel, R.; Xu, J.; Ward, E. Cancer statistics, 2010. *Ca A Cancer Journal for Clinicians* **2013,** 63, 11-30.

3. Siegel, R. L.; Miller, K. D.; Ahmedin Jemal, D. V. M. P. Cancer statistics, 2017. *Ca A Cancer Journal for Clinicians* **2017,** 67, 7–30.

4. Rudin, C. M.; Poirier, J. T.; Byers, L. A.; Dive, C.; Dowlati, A.; George, J.; Heymach, J. V.; Johnson, J. E.; Lehman, J. M.; MacPherson, D.; Massion, P. P.; Minna, J. D.; Oliver, T. G.; Quaranta, V.; Sage, J.; Thomas, R. K.; Vakoc, C. R.; Gazdar, A. F. Molecular subtypes of small cell lung cancer: a synthesis of human and mouse model data. *Nature reviews. Cancer* **2019,**19, 289-297.

5. Huang, Y.; Feng, Q. I.; Yan, Q.; Hao, X.; Chen, Y. Alpha-helical cationic anticancer peptides: a promising candidate of novel anticancer drugs. *Mini Reviews in Medicinal Chemistry* **2015,** 15, 73-81.

6. Wang, S. H.; Yu, J. Structure-based design for binding peptides in anti-cancer therapy. *Biomaterials* **2017,** 156, 1-15.

7. Fox, J. L. Antimicrobial peptides stage a comeback. *Nature Biotechnology* **2013,** 31, 379-382.

8. Kim, S.; Hyun, S.; Lee, Y.; Lee, Y.; Yu, J. Nonhemolytic cell-penetrating peptides: site specific introduction of glutamine and lysine residues into the α-helical peptide causes deletion of its direct membrane disrupting ability but retention of its cell penetrating ability. *Biomacromolecules* **2016,** 17, 3007-3015.

9. Ong, Z. Y.; Wiradharma, N.; Yang, Y. Y. Strategies employed in the design and optimization of synthetic antimicrobial peptide amphiphiles with enhanced therapeutic potentials. *Adv Drug Deliv Rev* **2014,** 78, 28-45.

10. Saxena, P.; Severi, L.; Santucci, M.; Taddia, L.; Ferrari, S.; Luciani, R.; Marverti, G.; Marraccini, C.; Tondi, D.; Mor, M. Conformational propensity and biological studies of proline mutated LR peptides inhibiting human thymidylate synthase and ovarian cancer cell growth. *Journal of Medicinal Chemistry* **2018,** 61, 7374-7380.

11. Oren, Z.; Lerman, J. C.; Gudmundsson, G. H.; Agerberth, B.; Shai, Y. Structure and organization of the human antimicrobial peptide LL-37 in phospholipid membranes: relevance to the molecular basis for its non-cell-selective activity. *Biochemical Journal* **1999,** 341 (Pt 3), 501-513.

12. Ciornei, C. D.; Sigurdardóttir, T.; Schmidtchen, A.; Bodelsson, M. Antimicrobial and chemoattractant activity, lipopolysaccharide neutralization, cytotoxicity, and inhibition by serum of analogs of human cathelicidin LL-37. *Antimicrobial Agents & Chemotherapy* **2005,** 49, 2845-2850.

13. Chen, C.; Yang, C.; Chen, Y.; Wang, F.; Mu, Q.; Zhang, J.; Li, Z.; Pan, F.; Xu, H.; Lu, J. R. Surface physical activity and hydrophobicity of designed helical peptide amphiphiles control their bioactivity and cell selectivity. *Acs Appl Mater Interfaces* **2016,** 8, 26501-26510.

14. Nan, Y. H.; Bang, J. K.; Jacob, B.; Park, I. S.; Shin, S. Y. Prokaryotic selectivity and LPS-neutralizing activity of short antimicrobial peptides designed from the human antimicrobial peptide LL-37. *Peptides* **2012,** 35, 239-247.

15. Zhang, P.; Ma, J.; Yan, Y.; Chen, B.; Liu, B.; Jian, C.; Zhu, B.; Liang, S.; Zeng, Y.; Liu, Z.

Arginine modification of lycosin-I to improve inhibitory activity against cancer cells. *Organic & Biomolecular Chemistry* **2017,** 15, 9379-9388.

16. Conde, J.; Bao, C.; Tan, Y.; Cui, D.; Edelman, E. R.; Azevedo, H. S.; Byrne, H. J.; Artzi, N.; Tian, F. Dual targeted immunotherapy via in vivo delivery of biohybrid RNAi-peptide nanoparticles to tumour-associated macrophages and cancer cells. *Advanced Functional Materials* **2015,** 25, 4183-4194.

17. Wang, C.; Howell, M.; Raulji, P.; Davis, Y.; Mohapatra, S. Preparation and characterization of molecularly imprinted polymeric nanoparticles for atrial natriuretic peptide (ANP). *Advanced Functional Materials* **2011,** 21, 4423-4429.

18. Lehto, T.; Vasconcelos, L.; Margus, H.; Figueroa, R.; Pooga, M.; Hällbrink, M.; Langel, U. Saturated fatty acid analogues of cell-penetrating peptide PepFect14: role of fatty acid modification in complexation and delivery of splice-correcting oligonucleotides. *Bioconjugate Chemistry* **2017,** 28, 782-792.

19. Yuan, H.; Fales, A. M.; Vo-Dinh, T. TAT peptide-functionalized gold nanostars: enhanced intracellular delivery and efficient NIR photothermal therapy using ultralow irradiance. *Journal of the American Chemical Society* **2012,** 134, 11358-11361.

20. Park, H.; Tsutsumi, H.; Mihara, H. Cell-selective intracellular drug delivery using doxorubicin and α-helical peptides conjugated to gold nanoparticles. *Biomaterials* **2014,** 35, 3480-3487.

21. Tan, H.; Huang, Y.; Xu, J.; Chen, B.; Zhang, P.; Ye, Z.; Liang, S.; Xiao, L.; Liu, Z. Spider toxin peptide Lycosin-I functionalized gold nanoparticles forin vivo tumor targeting and therapy. *Theranostics* **2017,** 7, 3168-3178.

22. Guo, J.; Hu, H.; Zhao, Q.; Wang, T.; Zou, Y.; Yu, S.; Wu, Q.; Guo, Z. Synthesis and antifungal activities of glycosylated derivatives of the cyclic peptide fungicide caspofungin. *Chemmedchem* **2012,** 7, 1496-1503.

23. Zhao, Q.; Zou, Y.; Guo, J.; Yu, S.; Chai, X. Y.; Hu, H.; Wu, Q. Synthesis and antifungal activities of N -glycosylated derivatives of tunicyclin D, an antifungal octacyclopeptide. *Tetrahedron* **2014,** 70, 7780-7787.

24. Taichi, U.; Kazuyoshi, T.; Yoshihide, N.; Takaomi, I.; Masataka, F.; Tomoaki, T.; Hirofumi, N.; Akio, T.; Shin-Ichi, M.; Hiroko, T. Chemoenzymatic synthesis of glycosylated glucagon-like peptide 1: effect of glycosylation on proteolytic resistance and in vivo blood glucose-lowering activity. *Journal of the American Chemical Society* **2009,** 131, 6237-6245.

25. Warburg, O. On the origin of cancer cells. *Science* **1956,** 123, 309-314.

26. Vander Heiden, M. G.; Cantley, L. C.; Thompson, C. B. Understanding the warburg effect: the metabolic requirements of cell proliferation. *Cancer Discovery* **2012,** 2, 881-898.

27. Cantor, J. R.; Sabatini, D. M. Cancer cell metabolism: one hallmark, many faces. *Cancer Discovery* **2012,** 2, 881-898.

28. Vander Heiden, M. G. Targeting cancer metabolism: a therapeutic window opens. *Nature Reviews Drug Discovery* **2011,** 10, 671-684.

29. Calvaresi, E. C.; Hergenrother, P. J. Glucose conjugation for the specific targeting and treatment of cancer. *Chemical Science* **2013,** 4, 2319-2333.

30. Patra, M.; Awuah, S. G.; Lippard, S. J. Chemical approach to positional isomers of glucose-platinum conjugates reveals specific cancer targeting through glucose-transporter mediated uptake in vitro and in vivo. *Journal of the American Chemical Society* **2016,**

138,12541-12551.

31. Patra, M.; Johnstone, T. C.; Suntharalingam, K.; Lippard, S. J. A potent glucose-platinum conjugate exploits glucose transporters and preferentially accumulates in cancer cells. *Angewandte Chemie* **2016,** 55, 2550-2554.

32. Zhang, P.; Zhang, E.; Xiao, M.; Chen, C.; Xu, W. Enhanced chemical and biological activities of a newly biosynthesized eugenol glycoconjugate, eugenol α-D-glucopyranoside. *Applied Microbiology & Biotechnology* **2013,** 97, 1043-1050.

33. Zasloff, M. Antimicrobial peptides of multicellular organisms. *Nature* **2002,** 415, 389-395.

34. Clogston, J. D.; Patri, A. K. Zeta potential measurement. *Methods Mol Biol* **2011,** 697, 63-70.

35. Zheng, M.; Yu, J. The effect of particle shape and size on cellular uptake. *Drug Delivery & Translational Research* **2016,** 6, 67-72.

36. Avrahami, D.; Shai, Y. Conjugation of a magainin analogue with lipophilic acids controls hydrophobicity, solution assembly, and cell selectivity. *Biochemistry* **2002,** 41, 2254-2263.

37. Chen, Y.; Mant, C. T.; Farmer, S. W.; Hancock, R. E. W.; Vasil, M. L.; Hodges, R. S. Rational design of α-helical antimicrobial peptides with enhanced activities and specificity/therapeutic index. *Journal of Biological Chemistry* **2005,** 280, 12316-12329.

38. Chen, Y.; Guarnieri, M. T.; Vasil, A. I.; Vasil, M. L.; Mant, C. T.; Hodges, R. S. Role of peptide hydrophobicity in the mechanism of action of alpha-helical antimicrobial peptides. *Antimicrob Agents Chemother* **2007,** 51, 1398-1406.

39. Hong, W.; Zhang, R.; Di, Z.; He, Y.; Zhao, Z.; Hu, J.; Wu, Y.; Li, W.; Cao, Z. Design of histidine-rich peptides with enhanced bioavailability and inhibitory activity against hepatitis C virus. *Biomaterials* **2013,** 34, 3511-3522.

40. Punj, V.; Bhattacharyya, S.; Saintdic, D.; Vasu, C.; Cunningham, E. A.; Graves, J.; Yamada, T.; Constantinou, A. I.; Christov, K.; White, B. Bacterial cupredoxin azurin as an inducer of apoptosis and regression in human breast cancer. *Oncogene* **2004,** 23, 2367-2378.

41. Szablewski, L. Expression of glucose transporters in cancers. *Biochim Biophys Acta* **2013,** 1835, 164-169.

42. Patra, M.; Johnstone, T. C.; Suntharalingam, K.; Lippard, S. J. A potent glucose-platinum conjugate exploits glucose transporters and preferentially accumulates in cancer cells. *Angewandte Chemie International Edition* **2016,** 55, 2550-2554.

43. Lee, T. H.; Hall, K. N.; Aguilar, M. I. Antimicrobial peptide structure and mechanism of action: a focus on the role of membrane structure. *Current Topics in Medicinal Chemistry* **2016,** 16, 25-39.

44. Dong, L.; Liu, Y.; Lu, Y.; Zhang, L.; Man, N.; Cao, L.; Ma, K.; An, D.; Lin, J.; Xu, Y. J. Tuning magnetic property and autophagic response for self-assembled Ni–Co alloy nanocrystals. *Advanced Functional Materials* **2013,** 23, 5930-5940.

45. Kerr, J. F.; Wyllie, A. H.; Currie, A. R. Apoptosis: a basic biological phenomenon with wide-ranging implications in tissue kinetics. *Br J Cancer* **1972,** 26, 239-257.

46. Green, D. R.; Reed, J. C. Mitochondria and apoptosis. *Science* **1998,** 281, 1309-1312.

47. Zhang, C.; Hu, R.; Huang, J.; Huang, X.; Shi, G.; Li, Y.; Yin, Y.; Chen, Z. Health effect of agricultural pesticide use in China: implications for the development of GM crops. *Scientific Reports* **2016,** 6, 34918.

48. Heiskanen, K. M.; Bhat, M. B.; Wang, H. W.; Ma, J.; Nieminen, A. L. Mitochondrial depolarization accompanies cytochrome c release during apoptosis in PC6 cells. *Journal of*

Biological Chemistry **1999,** 274, 5654-5658.

49. Chen, C.; Hu, J.; Zeng, P.; Pan, F.; Yaseen, M.; Xu, H.; Lu, J. R. Molecular mechanisms of anticancer action and cell selectivity of short α-helical peptides. *Biomaterials* **2014,** 35, 1552-1561.

50. Ashkenazi, A.; Dixit, V. M. Death receptors: signaling and modulation. *Science* **1998,**1305-1308.

51. Porter, A. G.; Jänicke, R. U. Emerging roles of caspase-3 in apoptosis. *Cell Death & Differentiation* **1999,** 6, 99-104.

52. Maria, V.; Sharon, G.; Frances, B.; Lisa, P.; Miriam, Z.; William, C.; Cara, L.; Marta, M.; David, H.; Eccles, S. A. Advances in establishment and analysis of three-dimensional tumor spheroid-based functional assays for target validation and drug evaluation. *BMC Biology,10,1(2012-03-22)* **2012,** 10, 29.

53. Hu, C.; Chen, X.; Huang, Y.; Chen, Y. Co-administration of iRGD with peptide HPRP-A1 to improve anticancer activity and membrane penetrability. *Scientific Reports* **2018,** 8, 2274.

54. Liu, J.; Liu, J.; Chu, L.; Zhang, Y.; Xu, H.; Kong, D.; Yang, Z.; Yang, C.; Ding, D. Self-assembling peptide of D-amino acids boosts selectivity and antitumor efficacy of 10-hydroxycamptothecin. *Acs Appl Mater Interfaces* **2014,** 6, 5558-5565.

55. Kaspar, A. A.; Reichert, J. M. Future directions for peptide therapeutics development. *Drug discovery today* **2013,** 18, 807-817.

56. Schweizer, F. Cationic amphiphilic peptides with cancer-selective toxicity. *Eur J Pharmacol* **2009,** 625, 190-194.

57. Gaspar, D.; Veiga, A. S.; Castanho, M. A. From antimicrobial to anticancer peptides. A

review. *Frontiers in microbiology* **2013,** 4, 294.

58. Riedl, S.; Zweytick, D.; Lohner, K. Membrane-active host defense peptides--challenges and perspectives for the development of novel anticancer drugs. *Chemistry and physics of lipids* **2011,** 164, 766-781.

59. Huang, Y.; Feng, Q.; Yan, Q.; Hao, X.; Chen, Y. Alpha-helical cationic anticancer peptides: a promising candidate for novel anticancer drugs. *Mini Rev Med Chem* **2015,** 15, 73-81.

60. Johnstone, S. A.; Gelmon, K.; Mayer, L. D.; Hancock, R. E.; Bally, M. B. In vitro characterization of the anticancer activity of membrane-active cationic peptides. I. Peptide-mediated cytotoxicity and peptide-enhanced cytotoxic activity of doxorubicin against wild-type and p-glycoprotein over-expressing tumor cell lines. *Anti-cancer drug design* **2000,** 15, 151-160.

61. Yang, C. Y.; Dantzig, A. H.; Pidgeon, C. Intestinal peptide transport systems and oral drug availability. *Pharmaceutical research* **1999,** 16, 1331-1343.

62. Zha, R. H.; Sur, S.; Stupp, S. I. Self-assembly of cytotoxic peptide amphiphiles into supramolecular membranes for cancer therapy. *Advanced healthcare materials* **2013,** 2, 126-133.

63. Yeaman, M. R.; Yount, N. Y. Mechanisms of antimicrobial peptide action and resistance. *Pharmacological reviews* **2003,** 55, 27-55.

64. Kahne, D.; Catherine Leimkuhler; Lu, W.; Christopher walsh. glycopeptide and lipoglycopeptide antibiotics. *Chemical Reviews* **2005,** 105, 425-448.

65. Yu, S. S.; Lau, C. M.; Thomas, S. N.; Jerome, W. G.; Maron, D. J.; Dickerson, J. H.; Hubbell, J. A.; Giorgio, T. D. Size- and charge-dependent non-specific uptake of PEGylated nanoparticles by macrophages. *International Journal of Nanomedicine* **2012,** 7, 799-813.

66. Makovitzki, A.; Fink, A.; Shai, Y. Suppression of human solid tumor growth in mice by intratumor and systemic inoculation of histidine-rich and pH-dependent host defense-like lytic peptides. *Cancer research* **2009,** 69, 3458-3463.

Table of Contents graphic

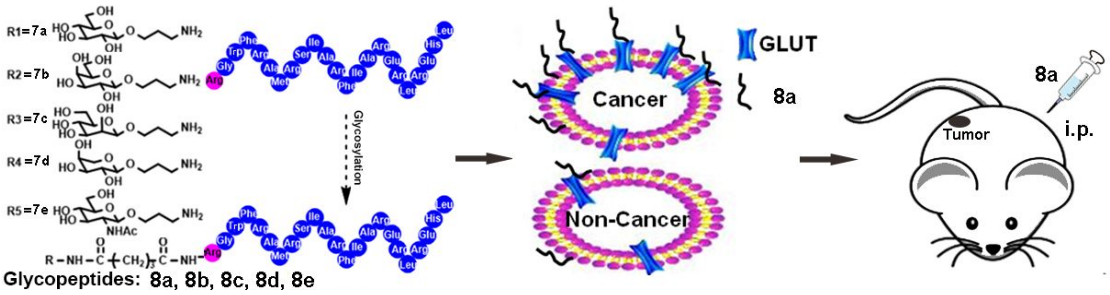
R1=7a
R2=7b
R3=7c
R4=7d
R5=7e
Glycosylation
Glycopeptides: 8a, 8b, 8c, 8d, 8e
Cancer
Non-Cancer
GLUT
8a
8a
Tumor
i.p.

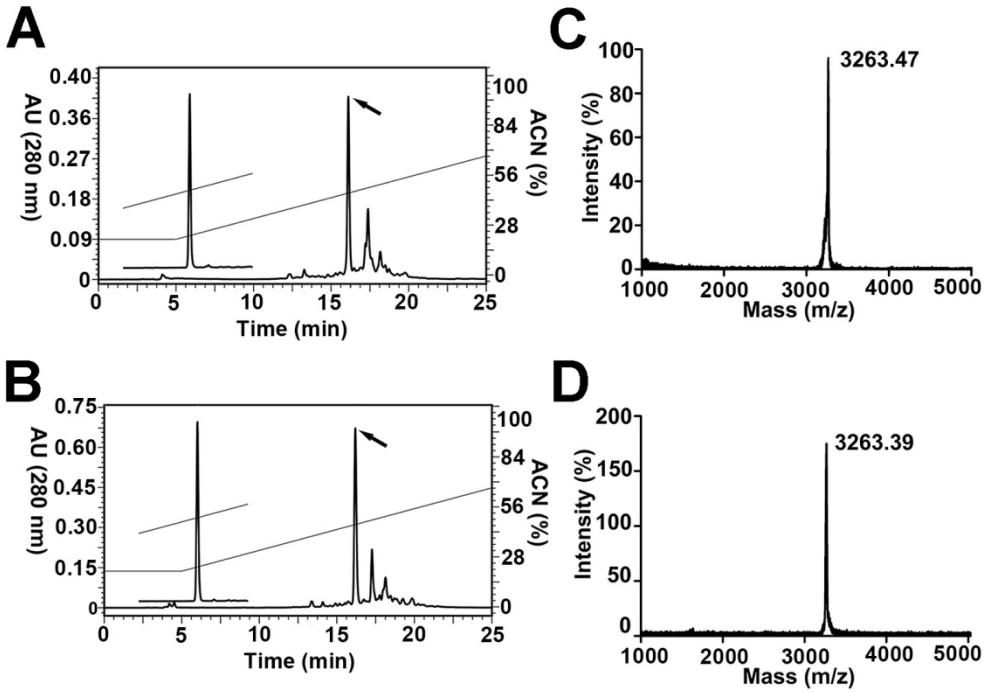

Figure 1. The purification and molecular mass determination of 8a and 8b.

160x114mm (254 x 254 DPI)

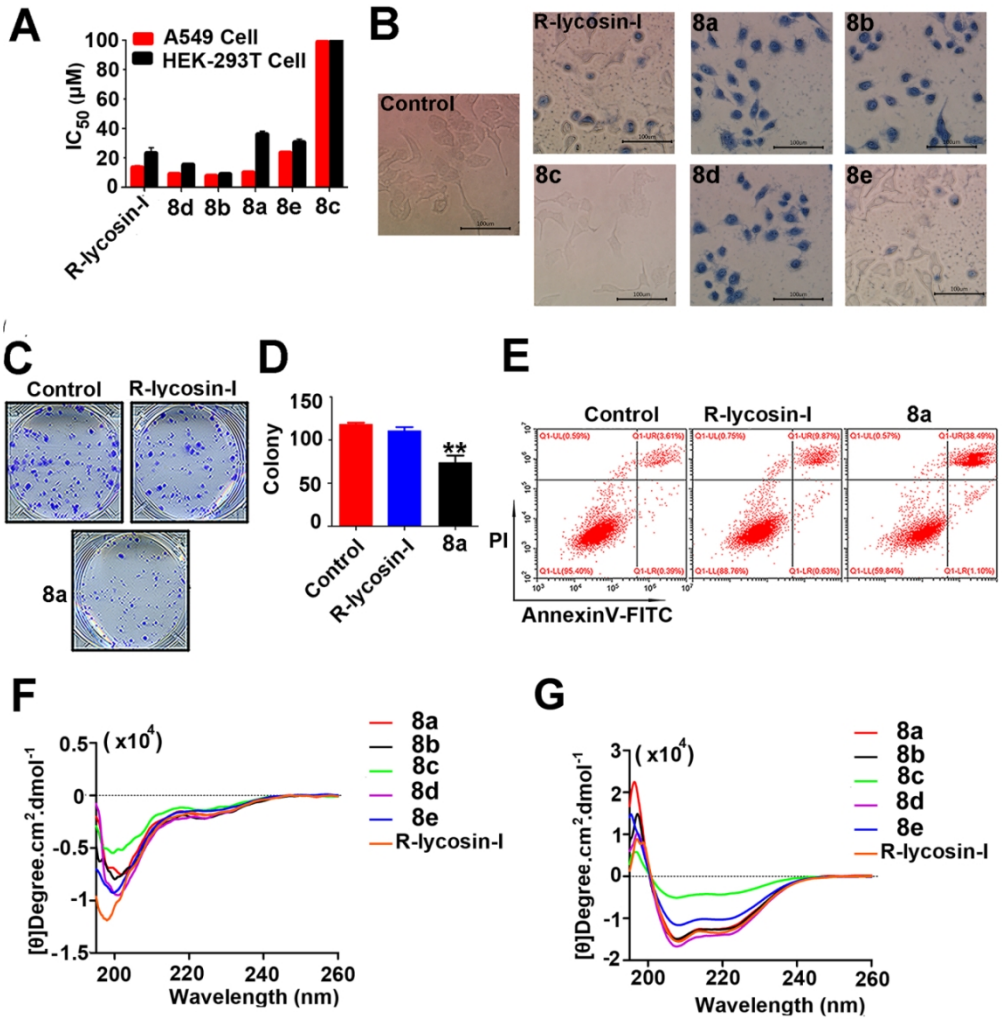

Figure 2. The cytotoxic activities of R-lycosin-I and five glycopeptides.

146x154mm (220 x 220 DPI)

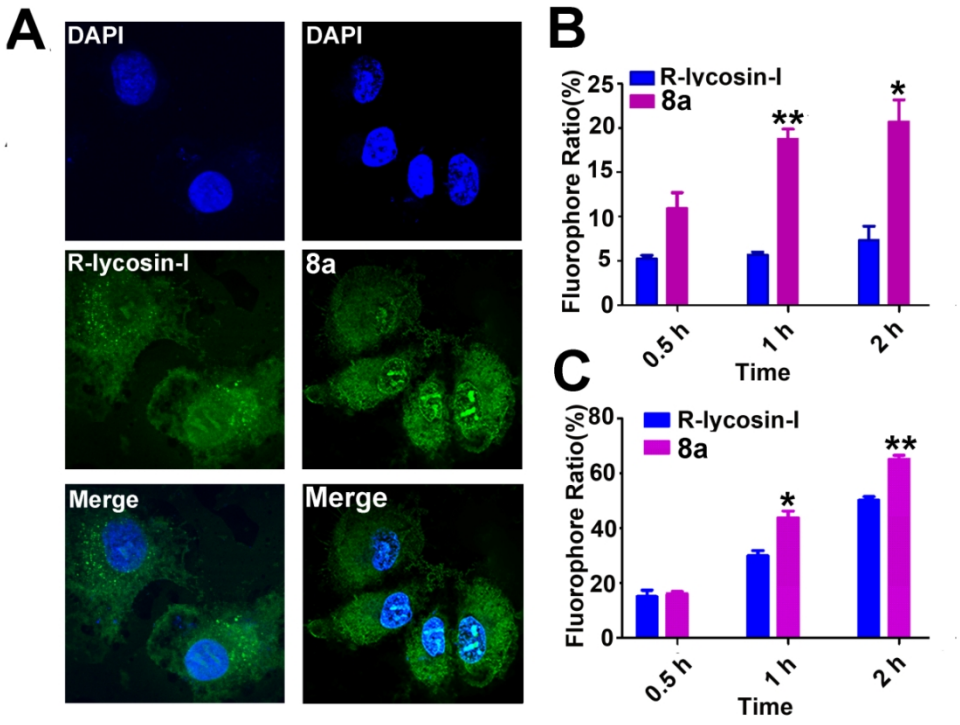

Figure 3. Cellular distribution and cell uptake ratio of R-lycosin-I and 8a.

146x104mm (220 x 220 DPI)

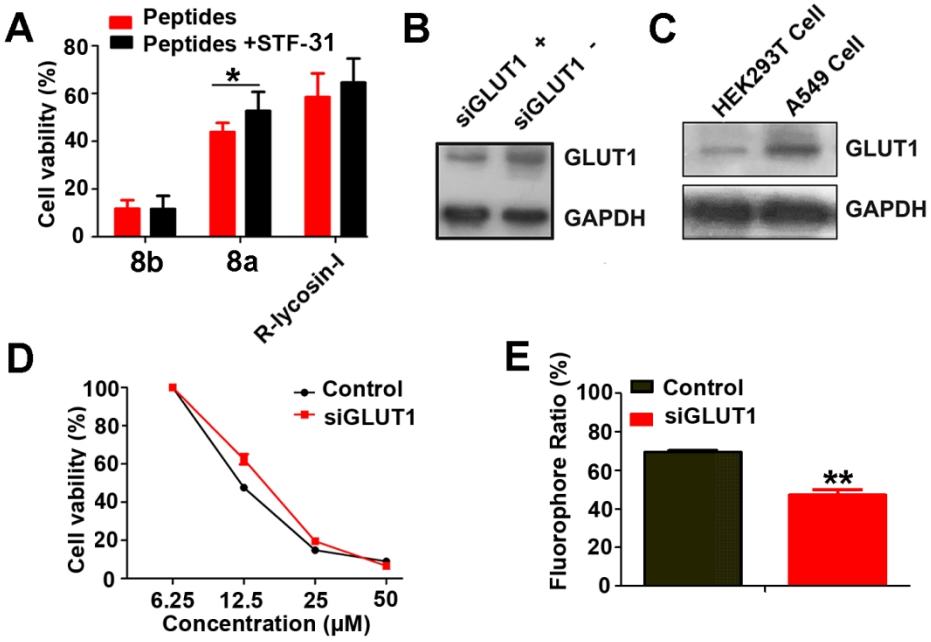

Figure 4. Glucose-transporter mediated cytotoxic activity of 8a

155x104mm (254 x 254 DPI)

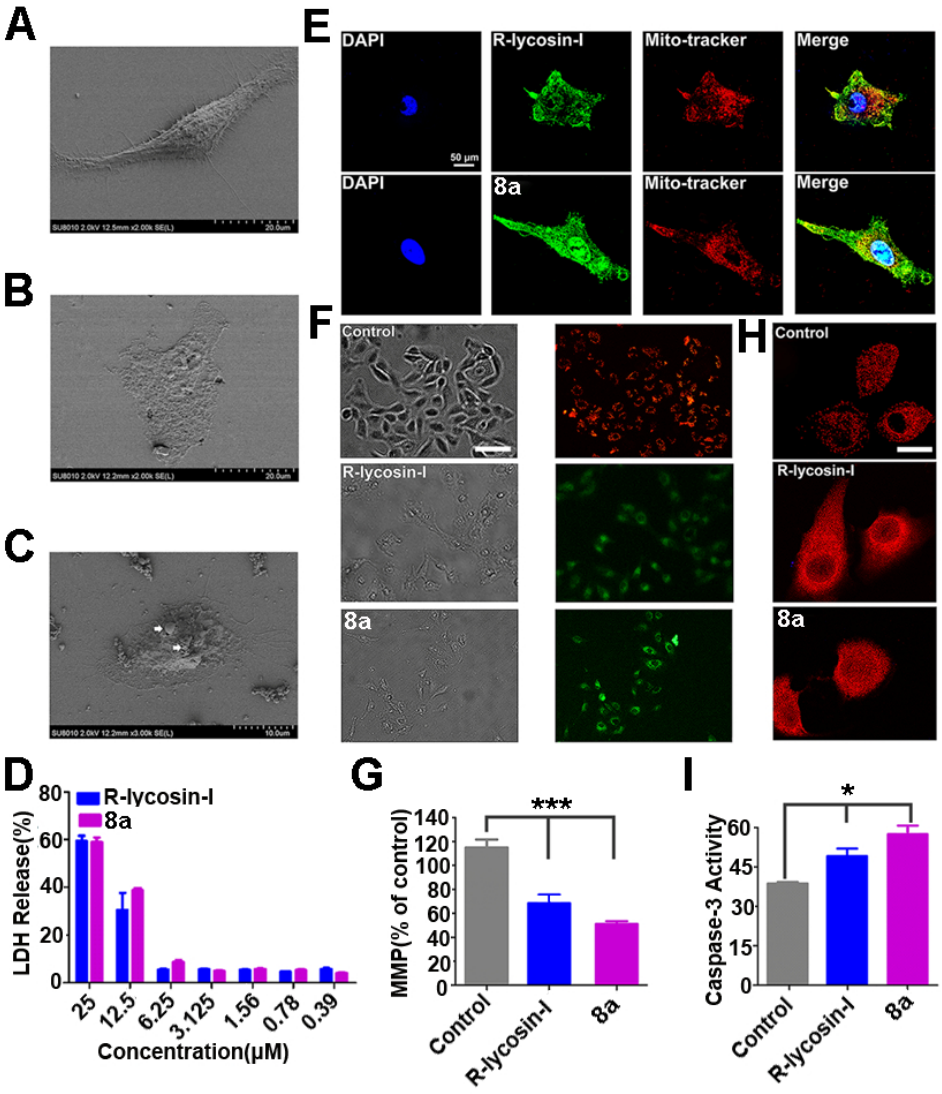

Figure 5. 8a caused direct cell membrane disruption and cell apoptosis.

229x257mm (96 x 96 DPI)

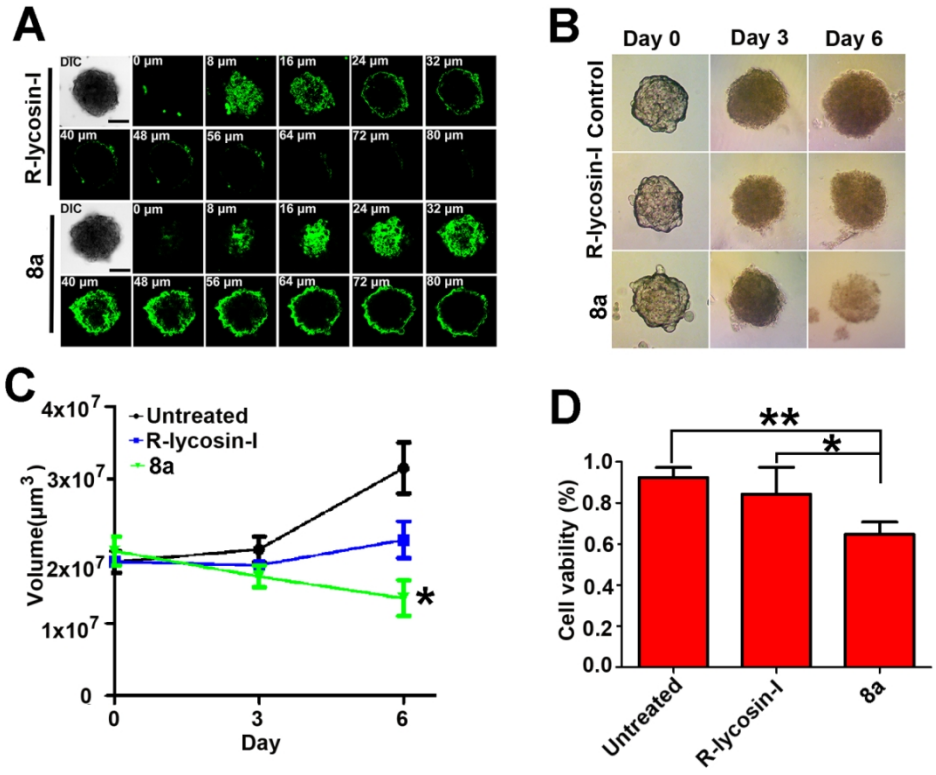

Figure 6. The effect of R-lycosin-I and 8a on the 3D tumor spheroids of A549 cells.

146x114mm (220 x 220 DPI)

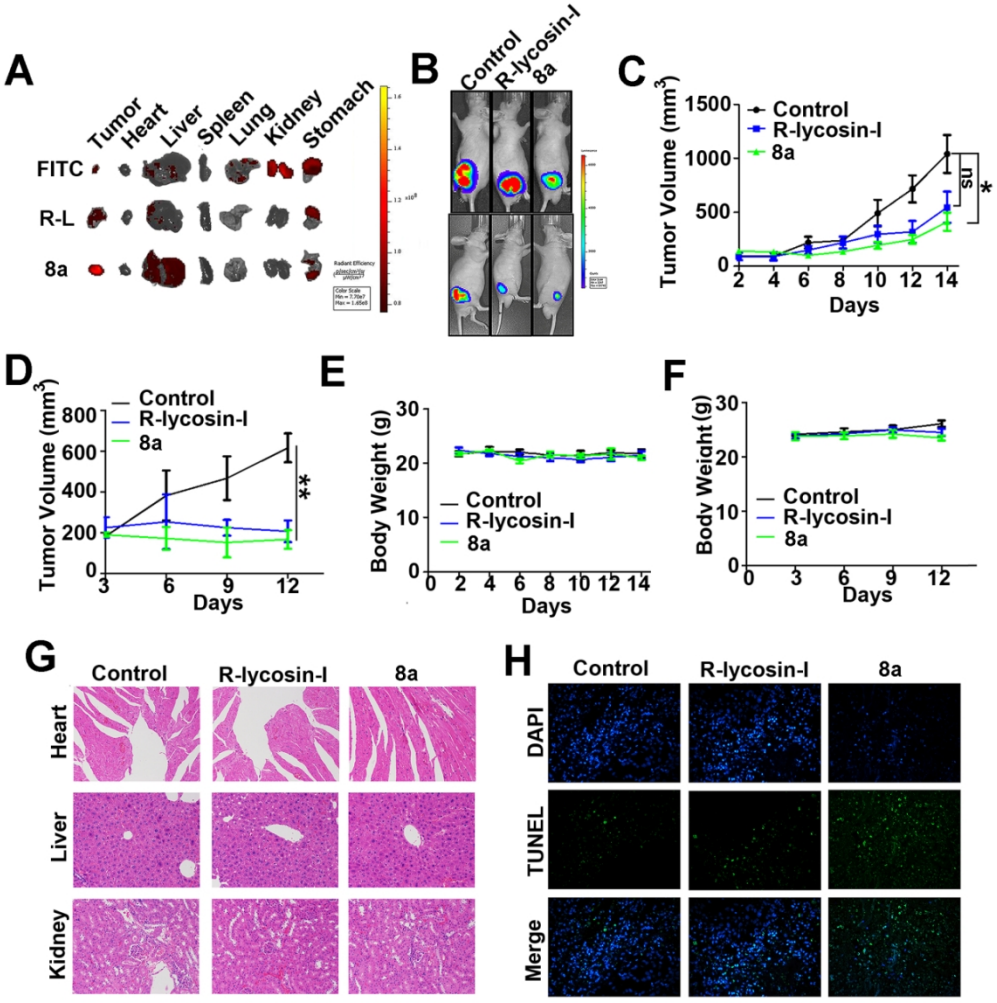

Figure 7. R-lycosin-I and 8a inhibited A549-luciferase tumor xenograft growth in vivo.

146x150mm (220 x 220 DPI)